Challenge Journal of
STRUCTURAL MECHANICS

Vol.7 No.4 (2021)

Mindlin's theory buckling compressive strength dynamic analysis dynamic response earthquake finite element analysis finite element method mechanical properties operational modal analysis optimization pushover analysis railways reinforced concrete seismic analysis seismic design seismic isolation shallow foundations steel silo teaching-learning based optimization th[illegible]iate

TULPAR ACADEMIC PUBLISHING

ISSN 2149-8024

Challenge Journal of Structural Mechanics

E-mail: *cjsmec@challengejournal.com*

Web page: *cjsmec.challengejournal.com*

TULPAR Academic Publishing
www.tulparpublishing.com

Challenge Journal of Structural Mechanics

CONTENTS

Research Articles

TULPAR ACADEMIC PUBLISHING

Challenge Journal of Structural Mechanics

Research Article

Design of cylindrical steel liquid tanks with stepped walls using One-foot method

Özer Zeybek [a,*]

[a] *Department of Civil Engineering, Muğla Sıtkı Koçman University, 48000 Muğla, Turkey*

ABSTRACT

Cylindrical steel tanks are used in most countries to store bulk volumes of both solid and liquid products such as water, oil, gasoline and grain. Such steel tanks are prone to buckling when subjected to external pressure either due to vacuum or due to wind. These types of shell structures are generally controlled by elastic buckling failure because of the thin wall thickness. Cylindrical shells are commonly constructed with stepwise variable wall thickness due to economic reasons. The thickness of the tank shell wall is designed to increase from top to bottom because the stress resultants on the tank wall gradually increase towards the base of the tank. For open-top tanks, a primary stiffening ring is required at or near the top to maintain roundness under all loads. Stress resultants in a primary stiffening ring were previously identified by the Author for uniform wall thick tanks. In this new study, the applicability of this hand calculation method in stepped wall tanks has been investigated. Pursuant to this goal, a specified tank shell was designed considering One-foot method. Then, the stepped wall tank was transformed into an equivalent 1-course tank for hand calculation. Using the previously developed hand calculation method by Author, a test for the in-plane bending moment in the ring was conducted to achieve an acceptable value for stepped wall tanks. The analysis results show that the previously proposed method for uniform wall thick tanks may also be used for stepped wall tanks considering an equivalent thickness. On the other hand, using Linear Buckling Analysis (LBA), the buckling mode was obtained for two different stepped wall tanks in the study.

ARTICLE INFO

Article history:
Received 20 July 2021
Revised 3 September 2021
Accepted 7 October 2021

Keywords:
Stepped wall tank
One-foot method
Primary stiffening ring
In-plane bending moment
Buckling

1. Introduction

Cylindrical steel tanks are used in most countries to store bulk volumes of both solid and liquid products such as water, oil, gasoline and grain. The thin wall makes the tank susceptible to buckling under external pressure due to wind, or partially vacuum when it is empty or partially emptied. Tank structures in the form of a cylindrical steel shell are generally controlled by elastic buckling failure because of the thin wall thickness. The behavior of the uniform wall thick tanks under environmental loads such as earthquake and wind has been explored by different research teams (Tedesco et al., 1989; Sivy and Musil, 2017; Chen and Rotter, 2012; Zdravkov, 2018; Zdravkov, 2019; Zeybek et al., 2019). However, the wall thickness of a storage tank is normally chosen to resist only the internal pressure from the stored product (Rotter et al., 2015). Instead of utilizing a uniform wall thickness, cylindrical shells of stepwise variable wall thickness are commonly constructed due to economic reasons.

As shown in Fig. 1, tank shell consists of a number of individual courses (also called strakes) each of constant thickness (Chen et al. 2011; Chen et al. 2012). The overall thickness of the tank wall is designed to increase from top to bottom because the stress resultants on the tank wall gradually increase towards the base of the tank (Chen et al., 2011, 2012).

* *Corresponding author*. Tel.: +90-252-211-2149 ; Fax: +90-252-211-1912 ; E-mail address: ozerzeybek@mu.edu.tr (Ö. Zeybek)
ISSN: 2149-8024 / DOI: https://doi.org/10.20528/cjsmec.2021.04.001

Nomenclature

θ	circumferential angle measured from the windward direction
CA	corrosion allowance (mm)
C_m	coefficient for each harmonic
D	tank diameter
G	design specific gravity of the liquid to be stored
H	height of the tank or maximum design liquid level
h_i	each course height
H_i	the distance from the top of the cylinder to the bottom of the i^{th} strake
I	an integer number of strakes
I_x	second moment of area normal to the plane of the ring
L	$(500Dt)^{0.5}$
l	half-wave-height of the buckle
m	harmonic number
M_x	in-plane bending moment of ring
n	total course number
N	total number of harmonics being considered
q	wind pressure on the stagnation meridian
S_d	allowable design condition stress (MPa)
S_t	allowable hydrostatic test condition stress (MPa)
t	bottom-course corroded shell thickness (mm)
t_{1d}	design shell thickness for bottom course (mm)
t_{1t}	hydrostatic test shell thickness for bottom course (mm)
t_d	design shell thickness (mm)
t_{eq}	equivalent uniform thickness
t_i	thickness of the i^{th} strake
t_t	hydrostatic test shell thickness (mm)
V	wind speed (km/h)
Z	section modulus of the ring (cm^3)
ν	Poisson's ratio
χ	shell-ring stiffness ratio

The top of the tank can be either fixed or open-topped. Open-top tanks require a stiffening ring at or near the top to maintain roundness under all loads. For a fixed-roof tank, the stiffening ring is not needed since the tank roof provides a natural restraint. According to API 650 (2013), there are three approaches to determine the required plate thickness of the tank shell. One of them is the One-foot method which is based on shell membrane theory (Azzuni and Guzey, 2015). The method computes the required thicknesses at design points 0.3 m above the bottom of each shell course. The One-foot method is used for tanks of less than 61 m in diameter. The second approach is the Variable-design-point method which was developed by Zick and McGrath (1968). According to API 650 (2013), the applicability of Variable-design-point method is limited by Eq. (1).

$$\frac{L}{H} \leq \frac{1000}{6} \tag{1}$$

The required plate thickness is determined by linear analysis for the tanks where the L/H ratio is more than 1000/6. However, API 650 (2013) does not describe a specific linear analysis method to calculate the plate thickness (Azzuni and Guzey, 2015).

The European standard for Shells EN 1993-1-6 (2007) allows transformation of stepped shell into equivalent uniform cylindrical shell considering a two-stage process. This approach based on the studies of Resinger and Greiner (1974, 1976) and Greiner (1981) includes complicated calculations that require interpolation. On the other hand, Chen et al. (2011) and Chen et al. (2012) proposed a new hand calculation method for stepped wall cylinders. Based on the research of Trahair et al. (1983), a simpler method was developed to get an equivalent uniform cylindrical shell.

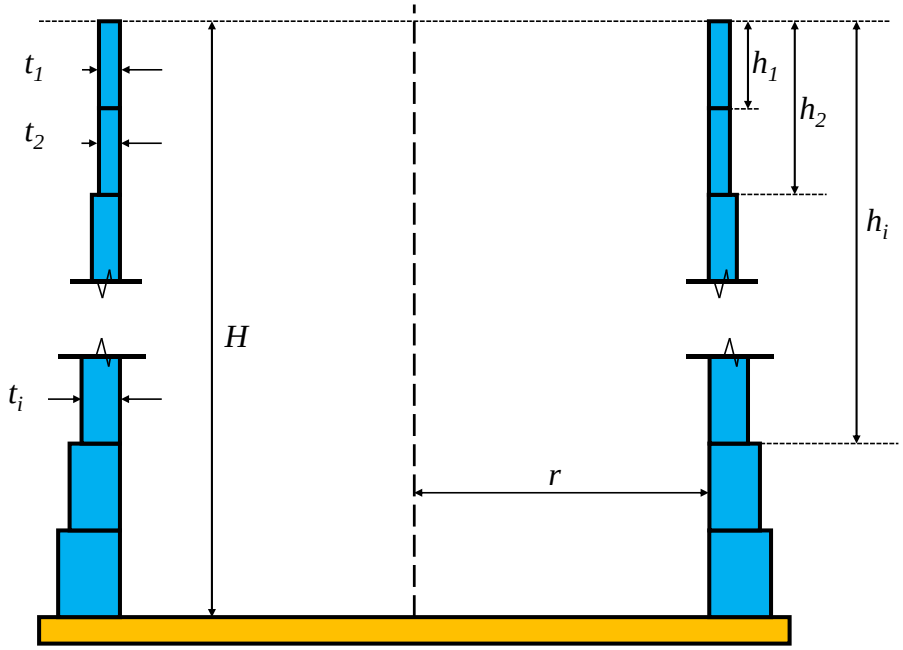

Fig. 1. Typical example of tank cross-section view (adopted from Chen et al. (2012)).

Moreover, an increase in the wall thickness is the one of the uneconomical ways to enhance the buckling resistance of the tank. To prevent this situation, a stiffening ring is placed at a suitable location to increase buckling resistance of the tanks (Rotter et al., 2015). Many researchers (Rotter et al., 2015; Bu and Qian, 2015; Bu and Qian, 2016; Dheyaaldın et al., 2017; Azzuni and Guzey, 2017; Sun et al., 2018; Zeybek et al., 2019; Zeybek and Seçer, 2020) conducted research for the sizing of such rings. For hand calculation, the step wall tank shell can be transformed into a 1-course equivalent tank shell as shown in Fig. 2.

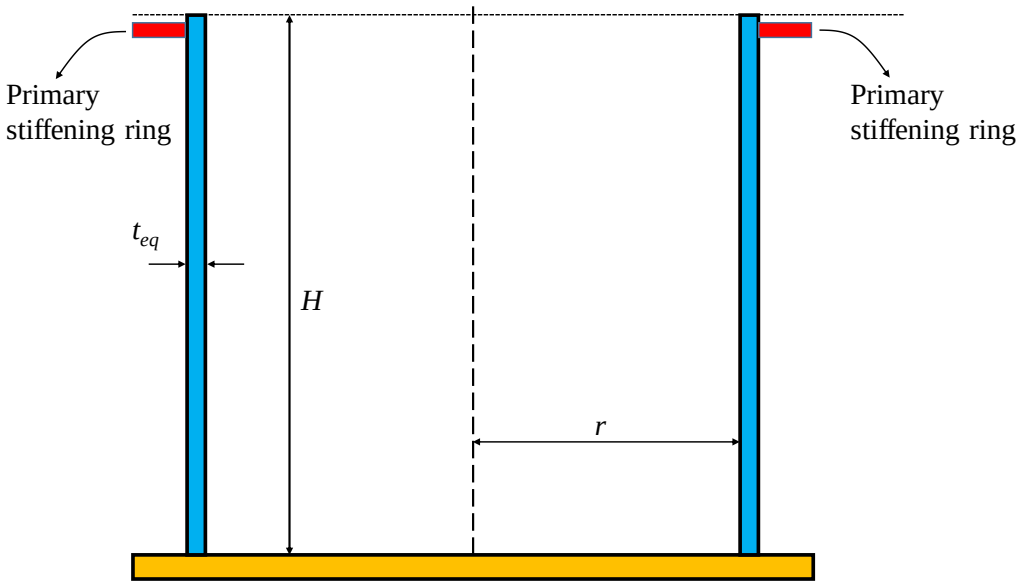

Fig. 2. Equivalent single cylinder of open-top tank with primary stiffening ring.

In this study, a tank shell wall was designed by considering the One-foot method. Then, the stepped-wall cylinder was transformed into an equivalent uniform cylindrical shell for hand calculation. After that, the size of the primary stiffening was determined by API 650 (2013) rules and in-plane bending moment variations were identified by the proposal of Zeybek et al. (2019). Moreover, the buckling mode of the specified stepped wall tanks under wind pressure was investigated by conducting Linear Bifurcation Analysis (LBA).

2. Tank Shell Wall Design Approaches

As mentioned before, three approaches have been proposed to calculate the shell thickness for storage tanks in the API 650 (2013) standard. The standard is used for the design of vertical, cylindrical, flat-bottomed and welded tanks. In this paper, these three approaches for shell design have been investigated in detail in the following sub-parts. It should be noted that below equations in the sub-parts are unit dependent. These equations in this study are in SI units.

2.1. The One-foot method

The One-foot method calculates the required plate thickness at design points 0.3 m above the bottom of each shell course. This method is valid for tanks of less than 61 m in diameter. According to API 650 (2013), the required minimum thickness of shell plates is obtained by considering the larger value calculated by the formulas below.

$$t_d = \frac{4.9\,D\,(H-0.3)\,G}{S_d} + CA \tag{2}$$

$$t_t = \frac{4.9\,D\,(H-0.3)}{S_t} \tag{3}$$

2.2. Variable-design-point method

The Variable-design-point method was proposed by Zick and McGrath (1968). It is used for tanks with the L/H ratio less than 1000/6. According to API 650 (2013), the required minimum thickness of shell plates is found by considering the larger value calculated by the formulas below.

$$t_{1d} = \left(1.06 - \frac{0.0696\,D}{H}\sqrt{\frac{H\,G}{S_d}}\right)\left(\frac{4.9\,H\,D\,G}{S_d}\right) + CA \tag{4}$$

$$t_{1t} = \left(1.06 - \frac{0.0696\,D}{H}\sqrt{\frac{H}{S_t}}\right)\left(\frac{4.9\,H\,D}{S_t}\right) \tag{5}$$

While calculating the second and upper shell courses, an iterative process is needed in the Variable-design-point method. However, there is no need for iteration in any stage of the One-foot method.

2.3. Linear analysis method

Linear analysis is used to calculate shell thickness of the tanks when One-foot method and Variable-design-point method are not permissible. It should be employed for the tanks where the L/H ratio is more than 1000/6.

However, traditional design treatments such as API 650 does not describe a specific linear analysis method to calculate the shell thickness. A recent study by Azzuni and Guzey (2015, 2016) proposed a rational analysis approach using thin shell theory. This approach also captures the plastic yielding moment of the bottom accurately when the tank exceeds limit value of 1000/6.

3. Transformation of Stepped Cylinder to Equivalent 1-Course Cylinder

The cylinder consisting of multiple sections with different wall thicknesses can be transformed into an equivalent 1-course cylinder. Chen et al. (2011) and Chen et al. (2012) developed a new hand calculation method for stepped wall cylinders. Based on the research of Trahair et al. (1983), a simple method was developed to get an equivalent uniform cylindrical shell. The new "weighted smeared wall method" was derived to find equivalent thickness. According to Fig. 1, the equivalent uniform thickness was given as follows:

$$t_{eq} = \left\{\left(\frac{1}{l}\right)\sum_{i=1}^{n}[t_i^3(H_i - H_{i-1})]\right\}^{1/3} \quad i = 1, 2, \ldots\ldots, n \quad (6)$$

in which $H_i = h_i - \frac{l}{2\pi}\, sin\frac{2\pi h_i}{l}$.

4. Calculation of the Primary Stiffening Ring Size

As shown in Fig. 3, there are many cross-sections for stiffening rings. These sections could be either from angle sections or formed from plates. Moreover, there are many design standards that recommend how the stiffening ring may be designed. The recommendations in the standards present a wide range of values for the ring size. There are two potential requirements (stiffness and strength) for the primary stiffening ring. One of the most common standards API 650 (2013) includes a strength design criteria for the ring. API 650 (2013) provides a section modulus (Z) according to a simplified mechanical model as follows:

$$Z = \frac{HD^2}{17}\left(\frac{V}{190}\right)^2 \quad (7)$$

According to Eq. (7), the required minimum section modulus is directly related to design wind speed, tank height and diameter.

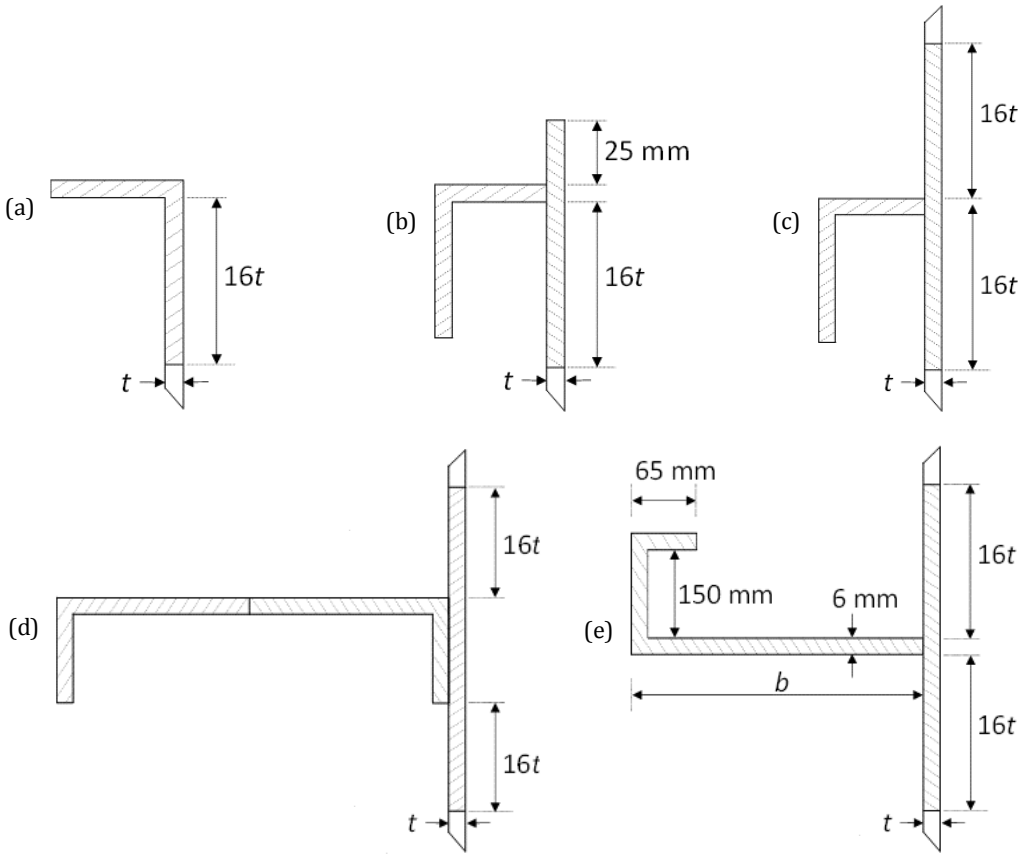

Fig. 3. Typical stiffening ring sections (adopted from API 650 (2013)):
a) Top angle; b) Curb angle; c) Single angle; d) Two angles; e) Formed plate.

A recent study by Zeybek et al. (2019) also proposed a strength criteria for the primary stiffening ring. In-plane bending moment (M_x) variation was identified considering a proposed shell-ring stiffness ratio (χ) and tributary height as follows:

$$M_x = -qr^2H\sum_{m=2}^{N}\frac{C_m f_2(x)}{(m^2-1)} f_1(x)\, cos\, m\theta \quad (8)$$

where

$$f_1(x) = a_1 + \frac{1}{(1+\chi)^{a_2}} \quad (9)$$

$$f_2(x) = \frac{a_3 \chi^{-a_5}}{a_4 + \chi^{-a_5}} \quad (10)$$

where constants a_1, a_2, a_3, a_4 and a_5 are given in Tables 1 and 2.

Table 1. Coefficients a_1 and a_2.

H/D	a_1	a_2
1.00	0.00001	0.98
0.75	0.00002	0.98
0.50	0.00003	0.95
0.25	0.00004	0.93

Table 2. Coefficients a_3, a_4 and a_5.

	m=2			m=3			m=4		
H/D	a_3	a_4	a_5	a_3	a_4	a_5	a_3	a_4	a_5
1.00	0.44	0.03	0.26	0.40	0.01	0.34	0.40	0.04	0.12
0.75	0.45	0.01	0.43	0.42	0.02	0.31	0.40	0.03	0.20
0.50	0.48	0.01	0.47	0.45	0.02	0.40	0.42	0.03	0.32
0.25	0.52	0.02	0.40	0.50	0.02	0.41	0.48	0.03	0.37

It should be noted above mentioned strength criteria was developed for uniform thick shells. In this study, the applicability of this approach will be investigated for stepped-wall tanks.

5. Numerical Study

Finite element analysis was used to evaluate two different tanks with stepped walls. In the first case, a tank diameter of 12 m and tank height of 12 m were selected with stepped thickness. The heights of the shell courses were 2.4 m. In the second case, a cylindrical tank with D=20 m and H=10 m was considered with stepped thickness. The heights of the shell courses were 2.5 m.

As shown in Fig. 4, thicknesses of the courses for both tank structures were computed as per API 650 (2013) using the One-foot method since the tank diameter is less than 61 m. S275 steel is used for the both tank models and the maximum allowable product design stress (S_d) was 167 MPa. The maximum allowable hydrostatic test stress (S_t) was 184 MPa as per Table 5.2a in API 650 (2013). The specific gravity of liquid was 1.0.

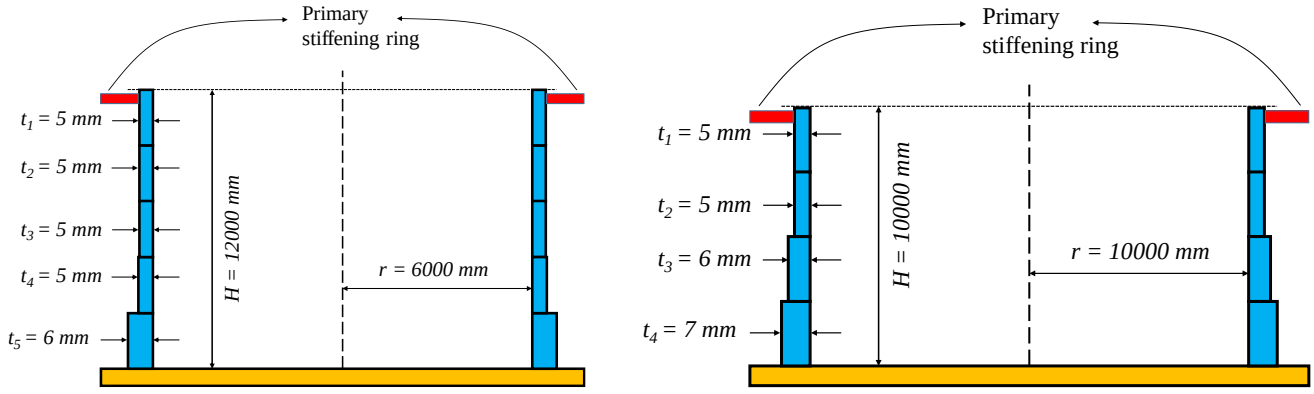

a) Case 1 b) Case 2

Fig. 4. Specific tank sections considered in numerical study.

The tank structures are considered open-top, so a primary stiffening ring is required at or near the top in order to maintain circularity when they are subjected to external pressure due to vacuum or wind. In this study, a primary stiffening ring is placed 200 mm away from the top of the tanks. The primary stiffening ring for both two cases is designed in accordance with API 650 (2013) with a design wind speed of 145 km/h. The required minimum section modulus for the rings was calculated ($Z_{required}$=59.2 cm^3 for Case 1 and $Z_{required}$=137.04 cm^3 for Case 2) considering Eq. (7). Unequal angles (100x75x7 for Case 1 and 150x100x10 for Case 2) were selected. According to the Table 5.20a in API 650 (2013), the provided section modulus ($Z_{provided}$) for Case 1 and Case 2 were 60.59 cm^3 and 155.91 cm^3 respectively. The selected unequal angle sections are shown in Fig. 5.

The commercial finite element program ANSYS was used to perform the numerical analysis. As shown in Fig. 6, half of the model is used and symmetry boundary conditions were applied to the nodes in each symmetry plane. Four-node shell elements (shell63) were used to model the cylindrical shell. The stiffening ring was modelled using two-node beam elements (beam4). The elas-

tic modulus was chosen as E=200 GPa and Poisson's ratio was chosen as ν=0.30. At the shell wall base, the nodes were restrained against all translational and rotational degrees of freedom (U_x=U_y=U_z=Rot$_x$=Rot$_y$ =Rot$_z$=0) to simulate a rigid bottom plate. A representative finite element mesh for two cases is shown in Fig. 6 where the line elements for the wind girder are shown in expanded form. It should be noted that wind forces act the numerical model and dynamic forces such as seismic effects were ignored in the study.

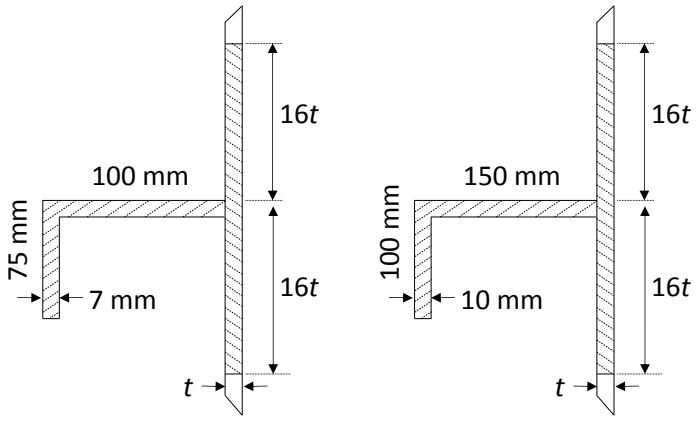

a) Case 1 b) Case 2

Fig. 5. Section of primary stiffening ring for Case 1 and Case 2.

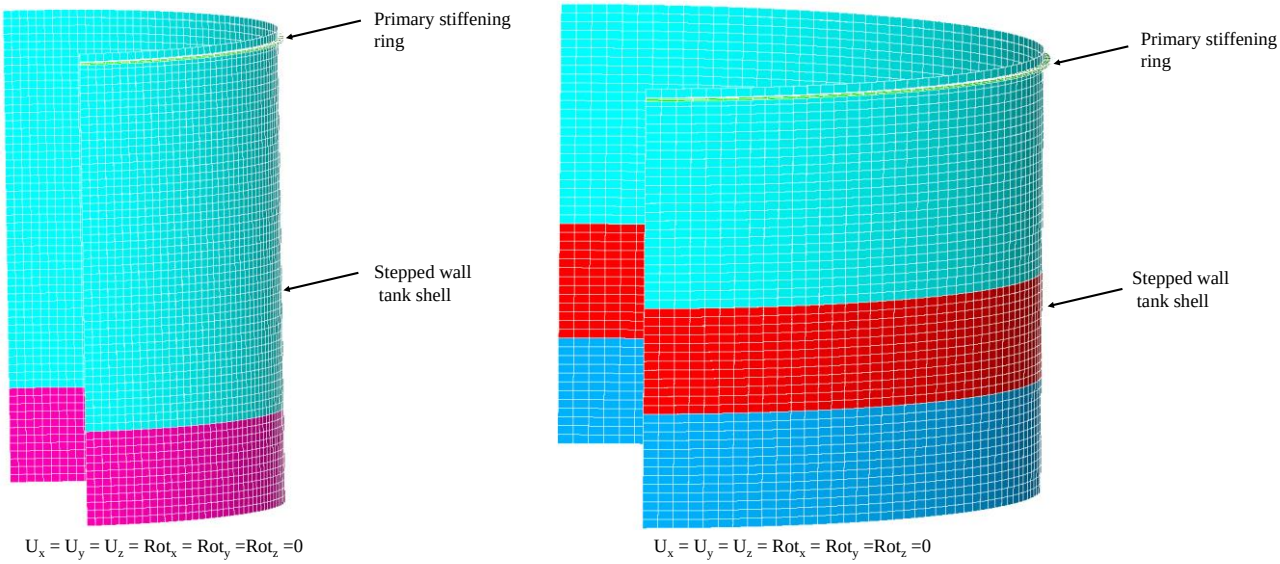

a) Case 1 b) Case 2

Fig. 6. FE models of the stepped wall tanks in numerical study.

Then considering the unequal angle section provided for the primary stiffening ring, the in-plane bending moment variation in the ring was calculated using Eq. (8). Since selected tank structures consist of stepped walls, an equivalent thickness is required for calculation of the in-plane bending moment. Eq. (6) was used for equivalent thickness.

For wind pressure distributions, Greiner terms (C_0=–0.55 for m=0, C_1=0.25 for m=1, C_2=1.0 for m=2, C_3=0.45 for m=3, C_4=-0.15 for m=4) were used. The empty cylindrical tank structures were subjected to a non-uniform wind pressure in the numerical study. Both numerical and hand calculation results for in-plane bending moment variations are shown in Fig. 7.

The comparison indicates that the proposal of Zeybek et al. (2019) provides an acceptable solution for the in-plane bending moment of the ring in two different specific stepped-wall tank structures; the estimated values are on the conservative side in the study.

On the other hand, Linear Bifurcation Analysis (LBA) was performed to get buckled shape of the specified stepped wall tank. LBA determines the elastic critical buckling resistance. Hence it can be a good first estimate of the elastic buckling strength of the tank structures. The buckled shape of the stepped wall tank structures under wind pressure was shown in Fig. 8. As seen in Fig. 8, the buckle form in windward side for the specific tanks extends almost over the whole height of the tank shell and it is more pronounced in the thinnest part.

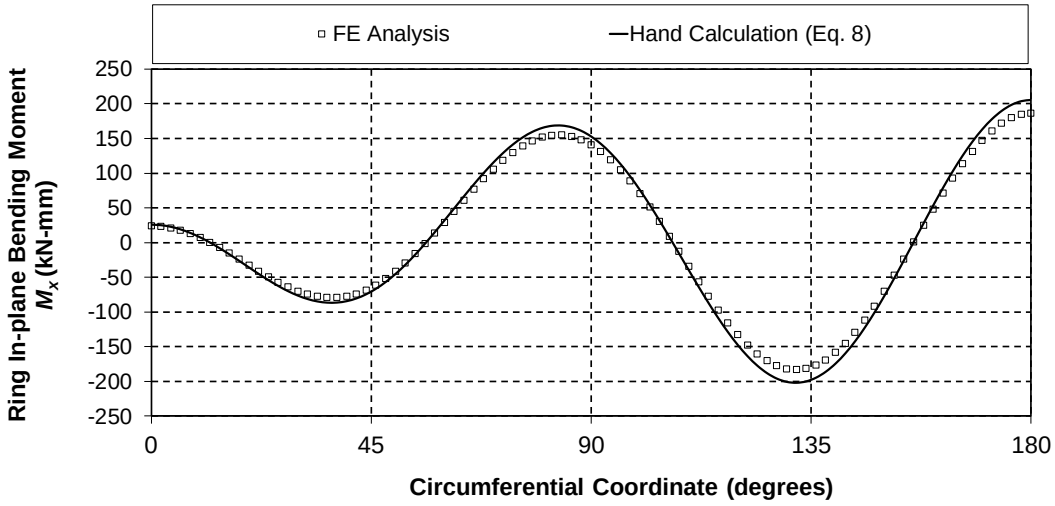

a) Case 1

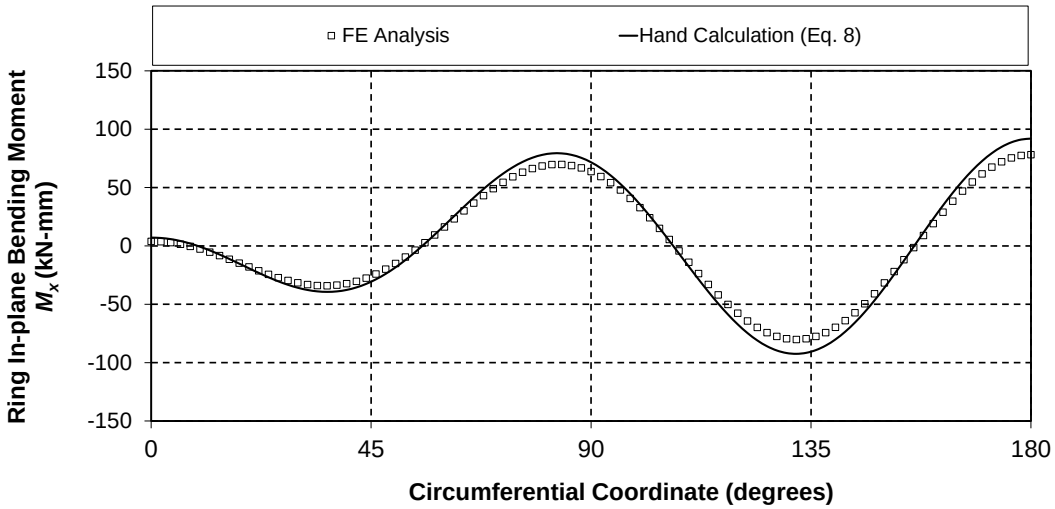

b) Case 2

Fig. 7. Comparison of hand calculation with FE values for the ring in-plane bending moment (M_x).

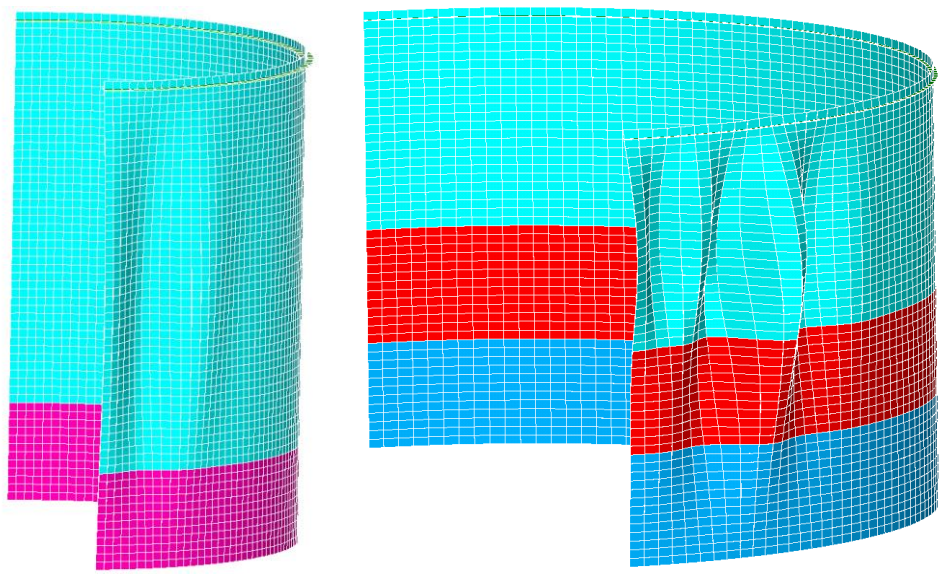

a) Case 1 b) Case 2

Fig. 8. Buckled shapes of the stepped wall tank models in numerical study.

6. Conclusions

This study presents the design of stepped wall storage tanks with primary stiffening rings according to API 650 (2013) rules. First, two tank structures were designed considering the One-foot method, which is one of the common tank shell design approaches. Then, the required section modulus was calculated considering design wind speed, tank height and diameter. Next, in order to investigate the applicability of the proposal of Zeybek et al. (2019) for in-plane bending moment in the stepped wall tank, the stepped tank shell was transformed into a 1-course equivalent tank shell using an approach which was given in Chen et al. (2011) and Chen et al. (2012).

Analysis results of the numerical examples show that the strength criteria developed by Zeybek et al. (2019) can also be applicable for stepped wall tanks that are designed with One-foot method. Moreover, buckled shapes of the two specific tank structures were obtained by conducting LBA. The buckle form in windward side for the tanks extends almost over the whole height of the tank shell and it is more pronounced in the thinnest part.

Future studies will concentrate on design requirements for large stepped wall tanks which are designed using the Variable-design-point method. The effect of secondary stiffening rings (also called intermediate rings) on tank behavior will be also investigated.

References

ANSYS (2010). Version 12.1 On-line User's Manual.

API 650 (2013). Welded tanks for oil storage (12th ed.), American Petroleum Institute, Washington, DC, USA.

Azzuni E, Guzey S (2015). Comparison of the shell design methods for cylindrical liquid storage tanks. *Engineering Structures*, 101, 621-630.

Azzuni E, Guzey S (2016). Design of cylindrical steel storage tanks: A linear elastic analysis approach. *Proceedings of the ASME 2016 Pressure Vessels and Piping Conference PVP2016,* Vancouver, British Columbia, Canada.

Azzuni E, Guzey E (2017). Stability of open top cylindrical steel storage tanks: design of top wind girder. *ASME Journal of Pressure Vessel Technology*, 139(3), 031207.

Bu F, Qian C (2015). A rational design approach of intermediate wind girders on large storage tanks. *Thin-Walled Structures*, 92, 76-81.

Bu F, Qian C (2016). On the rational design of the top wind girder of large storage tanks. *Thin-Walled Structures*, 99, 91-96.

Chen L, Rotter JM (2012). Buckling of anchored cylindrical shells of uniform thickness under wind load. *Engineering Structures*, 41, 199-208.

Chen L, Rotter JM, Doerich C (2011). Buckling of cylindrical shells with stepwise variable wall thickness under uniform external pressure. *Engineering Structures*, 33, 3570-3578.

Chen L, Rotter JM, Doerich-Stavridis C (2012). Practical calculations for uniform external pressure buckling in cylindrical shells with stepped walls. *Thin-Walled Structures*, 61, 2012, 162-168.

Dheyaaldın M, Özakça M, Dheyab A (2017). Effect of stiffeners on structural behavior of steel liquids tank. *The International Journal of Energy and Engineering Sciences*, 2(3), 0-0.

EN 1993-1-6 (2007). Eurocode 3 - Design of steel structures, Part 1.6: Strength and stability of shell structures. European Committee for Standardization, Brussels, CEN.

Greiner R (1981) Buckling of cylindrical shells with stepped wall thickness under wind load. *Der Stahlbau*, 1981, 50(6), 176-179.

Resinger F, Greiner R (1974). Zum beulverhalten von kreiszylinderschalen mit abgestufter wanddicke unter manteldruck. *Stahlbau*, 43, 182-187. (in German)

Resinger F, Greiner R (1976) Praktische beulberechnung oberirdischer zylindrischer tankbauwerke für unterdruck. *Stahlbau*, 45, 10-15. (in German)

Rotter JM, Kerr E, Lam HT, Holst JM (2015). Secondary rings for large tanks under external pressure. *8th International Conference on Advances in Steel Structures*, Lisbon, Portugal.

Sivy M, Musil M (2017). Seismic design of aboveground storage tanks containing liquid. *COMPDYN 2017 6th ECCOMAS Thematic Conference on Computational Methods in Structural Dynamics and Earthquake Engineering,* Rhodes Island, Greece.

Sun T, Azzuni E, Guzey S (2018). Stability of open-topped storage tanks with top stiffener and one intermediate stiffener subject to wind loading. *ASME Journal of Pressure Vessel Technology*, 140(1), 011204.

Tedesco JW, Landis, DW, Kostem CN (1989). Seismic analysis of cylindrical liquid storage tanks. *Computers & Structures*, 32(5), 1165-1174.

Trahair NS, Abel A, Ansourian P, Irvine HM, Rotter JM (1983). Structural design of steel bins for bulk solids. *Australian Institute of Steel Construction*, Sydney.

Zdravkov L (2018). Necessary height of the vertical stiffeners in steel silos on discrete supports. *Challenge Journal of Structural Mechanics*, 4(4), 153-158.

Zdravkov L (2019). Arch effect in silos on discrete supports - Is it a myth or reality? *Challenge Journal of Structural Mechanics*, 5(2), 72-79.

Zeybek Ö, Topkaya C, Rotter JM (2019). Stress resultants for wind girders in open-top cylindrical steel tanks. *Engineering Structures*, 196, 109347.

Zeybek Ö, Seçer M (2020). A design approach for the ring girder in elevated steel silos. *Thin-Walled Structures*, 157, 107002.

Zick LP, McGrath RV (1968). Design of large diameter cylindrical shells. *Proceeding Division Refining*, American Petroleum Institute New York, 48, 1114-1140.

Challenge Journal of Structural Mechanics

Research Article

Decision-making model based multilayer perceptrons for estimation of optimum design properties for truss structure

Melda Yucel [a], Gebrail Bekdaş [a,*], Sinan Melih Nigdeli [a]

[a] *Department of Civil Enginering, İstanbul University-Cerrahpaşa, 34320 İstanbul, Turkey*

ABSTRACT

Many branches of the structural engineering discipline have many problems, which require the generating an optimum model for beam-column junction area reinforcement, weight lightening for members such a beam, column, slab, footing formed as reinforced concrete, steel, composite, and so on, cost arrangement for any construction, etc. With this direction, in the current study, a structural model as a 5-bar truss is handled to provide an optimum design by determining the fittest areas of bar sections. It is aimed that the total bar length is minimized through population-based metaheuristic algorithm as teaching-learning-based optimization (TLBO). Following, the decision-making model is developed via multilayer perceptrons (MLPs) by performing an estimation application to enable directly foreseen of the optimal section areas and total length of bars, besides, the approximation and correlation success are evaluated via some metrics. Thus, determination of the real optimal results of unknown and not-tested designs can be realized with this model in a short and effective time.

ARTICLE INFO

Article history:
Received 30 August 2021
Revised 7 October 2021
Accepted 25 October 2021

Keywords:
Optimization
Metaheuristic algorithms
Teaching-learning based optimization
Truss structures
Multilayer perceptrons
Estimation

1. Introduction

Optimization is the process that is carried out to determine the most proper solution ways while reaching the results belonging to a problem, model, event, or case, or displaying the best performance intended for such elements. For this reason, the optimization concept can be accepted as betterment in a sense.

On the other side, in the optimum solution of any problem, reaching the determined aim or target function is necessitated various phases through fulfilling some conditions seen as required. However, the complexity of the problem precludes to search all kinds of possible solutions or solution combinations, and so, intended for the problem, to find good and proper solutions in an acceptable period, turns into the essential purpose. Nevertheless, in the designs consisted of numerous members, the mentioned optimization process may take long periods. In this regard, randomness and probabilistic situations in behaviors of heuristic and also metaheuristic approaches, which are a more advanced and differentiated version of heuristic ones, that one of the frequently used methods for optimization applications, can be a solution in terms of various applications and problems. If it is needed to give some examples to such design models, there are so many types of optimization processes realized to generate the most convenient and effective solutions with the help of various metaheuristics. For example, social spider optimization (SSO), enhanced colliding bodies optimization (ECBO), enhanced vibrating particles system (EVPS), particle swarm optimization (PSO), artificial bee colony (ABC), cuckoo search (CS), a hybrid version of butterfly optimization algorithm (BOA) and symbiosis organism search (SOS) algorithm, harmony search (HS), teaching-learning based optimization (TLBO), bat algorithm (BA) were used to find out the optimal structural design with minimizing the cost, weight, energy, CO_2 from greenhouse gases, etc. (Cakiroglu et al., 2021; Kaveh et al., 2020; Moayyeri et al., 2019; Öztürk, 2018; Sharma et al., 2021; Ulusoy et al., 2018; Ulusoy et al., 2020; Yucel et al., 2020). On the other hand, to create the best design and provide the suitable damping performance for vibration controlling systems such as base isolators, tuned mass dampers, active control mechanisms, etc., different

* *Corresponding author*. Tel.: +90-212-4737070 ; Fax: +90-212-4737180 ; E-mail address: bekdas@istanbul.edu.tr (G. Bekdaş)
ISSN: 2149-8024 / DOI: https://doi.org/10.20528/cjsmec.2021.04.002

methodologies among the mentioned algorithms were evaluated (Çerçevik et al., 2020; Hosseinaei et al., 2021; Lavasani and Doroudi, 2020; Nigdeli and Bekdaş, 2019; Vellar et al., 2019).

The fact remains, in time, it is clear that smart/intelligent techniques, which can reach the desired design criteria and solutions faster, and also have a measurable performance besides perform these actions in a short time and sensitively, replace these methods. The usage of these techniques avails in the sense of both time and spent effort, and thus, early intervention can come into question against negations arising in the designs.

The mentioned methods express the machine learning techniques taken place in artificial intelligence (AI) technology, and for any model, which has numerous design members, it can find out the results wished to be reached and determined, within an extremely short time. For example, in any city network line, pre-calculating how much the amount of water will give to occupants (Brentan et al., 2017; Lertpalangsunti et al., 1999; Msiza et al., 2008; Zubaidi et al., 2020); previously determination of the possibility of vehicular traffic accidents to may occur in any street, road, highway, urban area, etc. (Hu et al., 2004; Sikka, 2014; Wenqi et al., 2017); detection of the most proper dose of medicine for the treatment of any disease (Grossi et al., 2014; Huang et al., 2008; Huang et al., 2017; McDonald et al., 2015); foreseen of how much total construction cost of a structure, which will be made newly (Chakraborty et al., 2020; Koo et al., 2011; Magdum and Adamuthe, 2017; Shuitan et al., 2017), etc. In this regard, generation a combination of both techniques as optimization and machine learning, allow to users about some issues such as expediting of work wished to make, to be not required iteratively performing of intensive analyses, which necessitate long processes, to see quickly some results desired to forecast.

In the present study, a structural design as an optimization problem towards the determination of total bar length within a 5-bar truss model is tried to be solved by benefiting from teaching-learning-based optimization (TLBO). In this regard, optimum section areas of each bar are determined intended for achieving the minimum total length. Here, there is a case as different from classical optimization processes that some design parameters were handled in a specific range without a constant value to be used in the generation of decision-making model via multilayer perceptrons (MLPs), which is a kind of ANNs. Thanks to this, it becomes possible that target values are learned by the MLPs model via the generation of different design combinations intended for the truss model. Even, by this means, various controlling combinations, which are not handled and unknown previously, can be evaluated and directly detected through a developed learning model.

2. Background of Structural Optimization

Structural optimization is a highly important design problem for any engineer, analyzer, designer, etc. reposed in the civil engineering area, at the same time, it is accepted as a scientific discipline that is also studied by numerous researchers. The biggest reason for this importance is to may shine out numerous design combinations having different features, which can be acquired in the direction of factors such as used materials, labor applications, and especially, the defined design targets, etc. In this sense, the significant point is that the most optimum choice, which is a single one, is found to be discovered of design from among these many designs that it can perform the wished aim, and provides the required design conditions together with needs.

Furthermore, it is an important subject that in question determination of the most optimum option, namely what is tried to optimize in the process of optimization of parameters belonging to the design model. The most considerable issue is to be realized of the defined purpose. For instance, minimizing of the displacement values, which can occur in the design of a beam, column, retaining wall etc., establishment of a base isolation system exposing the cost in minimum level, modeling of a retaining wall, which has optimum design properties in the way of keeping CO^2 emission at the lowest degree, can be the major purpose of the designer. However, there is an important second issue that is analysis time and effort amount spent, and addition to these, also usually outlays, in the most proper level while trying to reach to basic purpose in the optimization process. Forwhy, optimization analyses conducted for some design problems take so long times, even a few weeks, and these causes to be not obtained of the desired results immediately in the awaited period. In this sense, it is extremely clear that new and advanced techniques are needed that they can be equal to optimization methods or work collaboratively with these, and thus make sensitive observations and give results in a short time comparing the usage of only optimization. The techniques, which can remove the mentioned disadvantages and provide these effects, are artificial intelligence and machine learning methods.

Accordingly, in structural engineering problems, it is seen that the mentioned methods, which have optimizing capability for such analyses and designs in the context of time, required exertion, are frequently utilized nowadays in terms of supporting optimization processes. For the sake of example to one of these; in the year 2017, a combination of particle swarm optimization (PSO) and bat algorithm (BA) metaheuristics is generated to create a seismically-optimized design for steel frame structures resisted to moment effects, and a model called as wavelet back-propagation neural networks were used for estimating of responses to control the limit state constraints (Gholizadeh and Mohammadi, 2017). Besides, by Xia et al. (2017), the support vector regression (SVR) technique is trained with the usage of genetic algorithm (GA) to detect the optimal parameters specific to SVR to determine damping ratios of cantilever beams by using this generated model. As to the other study, Torkan and Naderi Dehkordi (2018) carried out a study that consists of generation of several combinations, which are based on adaptive neuro-fuzzy inference system (ANFIS), SVR, and ANNs with PSO, to be able to determine the optimal algorithm parameters to estimate of concrete compressive strengths. Yaseen et al. (2018) predicted the shear strength values of steel fiber

reinforced concrete beams by considering SVR, and also ANNs, which are utilized with PSO. Also, the applied study is related to optimization of section sizes of steel tubular column model in the direction of achievement to the minimum cost. In this regard, one of the metaheuristic algorithms as flower pollination algorithm (FPA) is combined with multilayer artificial neural networks (ANNs) (Yucel et al., 2018). Additionally, values of dynamic increase factor parameter are determined via an ensemble algorithm as random forest hybridized with firefly algorithm (FA) intended to concrete structures reinforced with steel fiber material (Yang et al., 2019). Zhang et al. (2020) generated a combination for modeling optimum mixture proportions of concretes in the direction of that several machine learning techniques such as random forest, SVR, back-propagation ANNs are collaborated with PSO, respect to arranging of parameters of them. On the other hand, by Yücel et al. (2020a), the evaluation of generalized formulations developed for optimum tuned mass damper (TMD) parameters (f and ξ) is made, that they were proposed previously by using artificial neural networks (ANNs), which were combined with FPA to generate an optimum design of TMD to reduce of the floor responses as displacement and acceleration. Esfandiari and Urgessa (2020) proposed a hybrid model, which is comprised of decision-maker technique and PSO to generate an optimized model for reinforced concrete frames under the case of progressive collapse, too. Moreover, Ly et al. (2020) proposed two different models to estimate the ultimate shear capacities of steel fiber reinforced concrete beam structures. Here, the first and second analysis models are created depending on ANNs, which were arranged with GA and FA, respectively. Except all of these studies, several different optimized structural models are seen where various metaheuristic algorithms as FPA, harmony search (HS), and Jaya algorithm (JA) are benefited and combined via several machine learning techniques containing ANNs, bagging as an ensemble model, and random tree (Yücel et al., 2020b, 2020c).

3. Optimum Structural Design of 5-bar Truss Model

The optimum design model is based on a truss structure, which was consisted of five bar members, and can be seen in Fig. 1(a-b) together with a half-symmetric form belonging to this model. Due to the system is symmetrical, the truss structure can be analyzed and solved with the situation expressed in Fig. 1(b) as a half system.

Material elastic modulus (E) defined for each bar member of truss is 200000 MPa. As to the section areas (A) that belong to bars, is described as 100 mm^2, too. Also, loads, which are applied on the 1st and 2nd nodes taken place in the system, are 100 kN (P_2) and 50 kN (P_2), respectively, besides that the length of the span between supports (L) is 1000 mm.

The principal target in the problem is to find optimum namely the most convenient θ_1 and θ_2 design variable values that enable to minimize the total length of bars within the system. As a mathematical expression of the objective function of the problem, which is based on the mentioned design variables, is denoted via Eq. (1).

$$Min\ Total\ Length = Min\ f\ (\theta_1, \theta_2) = \sum_{i=1}^{3} L_i \quad (1)$$

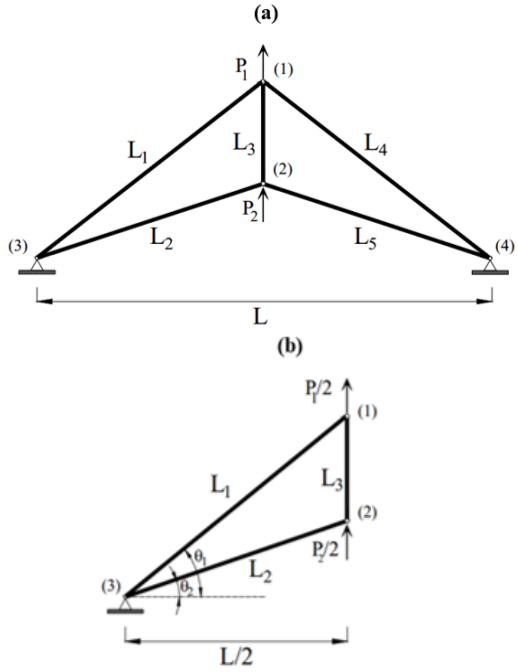

Fig. 1. 5-bar truss model: (a) schema of classical system; (b) half symmetric system (Majid, 1974).

Lengths of L_1, L_2 and L_3 bars that indicated as L_i in the equation, can be obtained by utilizing over geometric relations taken place in Eqs. (2-4), respectively.

$$L_1 = \frac{L}{2\cos(\theta_1)} \quad (2)$$

$$L_2 = \frac{L}{2\cos(\theta_2)} \quad (3)$$

$$L_3 = \frac{L_1}{\cos(\theta_2)}\sqrt{\cos^2(\theta_1) + cos^2(\theta_2) - 2\cos(\theta_1)\cos(\theta_2)\cos(\theta_1 - \theta_2)} \quad (4)$$

For design variables (θ) within the problem, lower ($\theta_{\min}$) and upper ($\theta_{\max}$) limit values determined in literature, can be expressed with Eq. (5).

$$0 < \theta < \frac{\pi}{3} \quad (5)$$

Additionally, in optimization application, which will be performed between these limits, vertical displacements that may occur on the 1st and 2nd nodes of the system (Δ_1 and Δ_2), are describes as design constraints, besides that these values can be provided via Eqs. (6) and (7), respectively. The upper bound of displacements (MaxΔ), which may emerge, is designated as 5 mm.

$$|\Delta_1(\theta_1, \theta_2)| \leq \max\Delta \quad (6)$$

$$|\Delta_2(\theta_1, \theta_2)| \leq \max\Delta \quad (7)$$

To define the problem in this stage, according to the maximum vertical displacement condition, which may occur in nodal points, optimization is the operation that finds of combination belonging to the most proper values of θ_1 and θ_2 angles, which remains in between 0 and

$\pi/3$ limits and will make a minimum of total length of bars within the system. Displacements of the mentioned nodal points can be detected by utilizing $K\Delta = P$ expression as static equilibrium equation. In the equation, K, Δ and P correspond to stiffness matrix, displacement vector and load vector in global coordinates, respectively. Here, K can be found via $B^T kB$ in the offing that B is transformation matrix (Eq. (8)) and k is stiffness matrix in local coordinates (Eq. (9)), where, B^T expresses the transpose of the transformation matrix.

$$B = \begin{bmatrix} \sin(\theta_1) & 0 \\ 0 & \sin(\theta_2) \\ 1 & -1 \end{bmatrix} \tag{8}$$

$$k = \begin{bmatrix} \frac{EA}{L_1} & 0 & 0 \\ 0 & \frac{EA}{L_2} & 0 \\ 0 & 0 & \frac{EA}{L_3} \end{bmatrix} \tag{9}$$

Eq. (10) is obtained for K when Eqs. (8) and (9) are substituted in the static equilibrium equation. And following, unknown displacement terms also can be found easily from $K\Delta = P$ equilibrium via Eq. (11).

$$K = EA \begin{bmatrix} \frac{\sin^2(\theta_1)}{L_1} + \frac{1}{2L_3} & -\frac{1}{2L_3} \\ -\frac{1}{2L_3} & \frac{\sin^2(\theta_2)}{L_2} + \frac{1}{2L_3} \end{bmatrix} \tag{10}$$

$$EA \begin{bmatrix} \frac{\sin^2(\theta_1)}{L_1} + \frac{1}{2L_3} & -\frac{1}{2L_3} \\ -\frac{1}{2L_3} & \frac{\sin^2(\theta_2)}{L_2} + \frac{1}{2L_3} \end{bmatrix} \begin{bmatrix} \Delta_1 \\ \Delta_2 \end{bmatrix} = \begin{bmatrix} \frac{P_1}{2} \\ \frac{P_2}{2} \end{bmatrix} \tag{11}$$

As additional information in these structural optimization processes, the number of population as a class comprised of students is handled as 20, besides that iteration number, in other words, total cycles or termination criteria performed for achieving to the optimum design is accepted as 10000.

4. Teaching-Learning Based Optimization (TLBO)

In the year 2011, teaching-learning based optimization (TLBO), which is a population-based metaheuristic algorithm, is improved by Rao et al. (2011) based on the teaching effect of a teacher on students within the class, and interaction together with the transfer of knowledge between students each other as the resultant of this learning. In this algorithm, which is proposed in the direction of consideration two separate phases as teacher and student, besides that community i.e. population (sn) is a class where many students exist, each candidate solution in the optimization process for j=1, 2,..., sn is represented by a student. In addition to this, a teacher is assumed and selected as the most informed/experienced person about an issue among all students in the class (Rao et al., 2011). In this regard, training of students is realized by the teacher (Eq. (12)), which is defined as the best solution in the first stage, and here, improvement of knowledge level and mean results for a specific subject of all students are provided that teacher conveys own information to other students in a specific rate known as teaching factor (TF) (Rao et al., 2011; Rao, 2016).

$$X_{i,\text{new}} = X_{i,j} + \text{rand}\,(\,)\left(X_{i,g_{\text{best}}} - (TF)\,X_{i,\text{mean}}\right) \tag{12}$$

$$TF = \text{round}\left(1 + \text{rand}\,(\,)\right) \tag{13}$$

In the duration of the student phase, two different solutions (n and m) are selected as randomly among all students that improving knowledge level, and this level is updated again as expressed in Eq. (14) based on objective function value (in case minimization of the problem) (Rao, 2016). The expressions with descriptions of optimization members and algorithm parameters are given in Table 1.

$$X_{i,\text{new}} = \begin{cases} OF_n < OF_m, & X_{i,j} + \text{rand}\,(\,)\left(X_{i,n} - X_{i,m}\right) \\ OF_n > OF_m, & X_{i,j} + \text{rand}\,(\,)\left(X_{i,m} - X_{i,n}\right) \end{cases} \tag{14}$$

Table 1. Expressions with descriptions of optimization members and algorithm parameters.

Property	Notation	Description/Task
User-defined coefficient	sn	Number of all students as candidate solutions / Total population number within solution matrix
Member of process	$X_{i,\text{new}}$	The determined new solution value for i^{th} design variable
	$X_{i,j}$	Initial matrix value of j^{th} candidate solution namely student belong to i^{th} design variable
	$X_{i,g_{\text{best}}}$	The value of i^{th} design variable belong to the best solution (defined as teacher member) in terms of objective function quality
	$X_{i,\text{mean}}$	Mean value of all candidate solution values belonging to i^{th} design variable
	$X_{i,n}$	The value of i^{th} design variable for n^{th} candidate solution randomly-selected from initial matrix
	$X_{i,m}$	i^{th} design variable value of m^{th} candidate solution randomly-selected from initial matrix
	OF_n	Objective function value belonging n^{th} candidate solution
	OF_m	Objective function value belonging m^{th} candidate solution
Used functions in optimization application	rand ( )	A random number generating function between 0 and 1
	round ( )	Function that it rounds decimal number in parenthesis to closest integer number
	mean ( )	Function provides that averaging of member values within a specific number array
	min ( )	Function determining of the minimum one among values in certain amount

In the present study, the main purpose of using TLBO is that the algorithm provides the randomization and thus successfully optimization for design variables in the way of realizing the objective of the problem. The reason for this case is based on that TLBO has two different and sequential phases, which are producing the solutions by evaluating the best members and considering all of the population. In this respect, the optimization process can be carried out in two individual stages by handling the possibility of different solutions. Also, the flowchart of TLBO algorithm can be seen in Fig. 2.

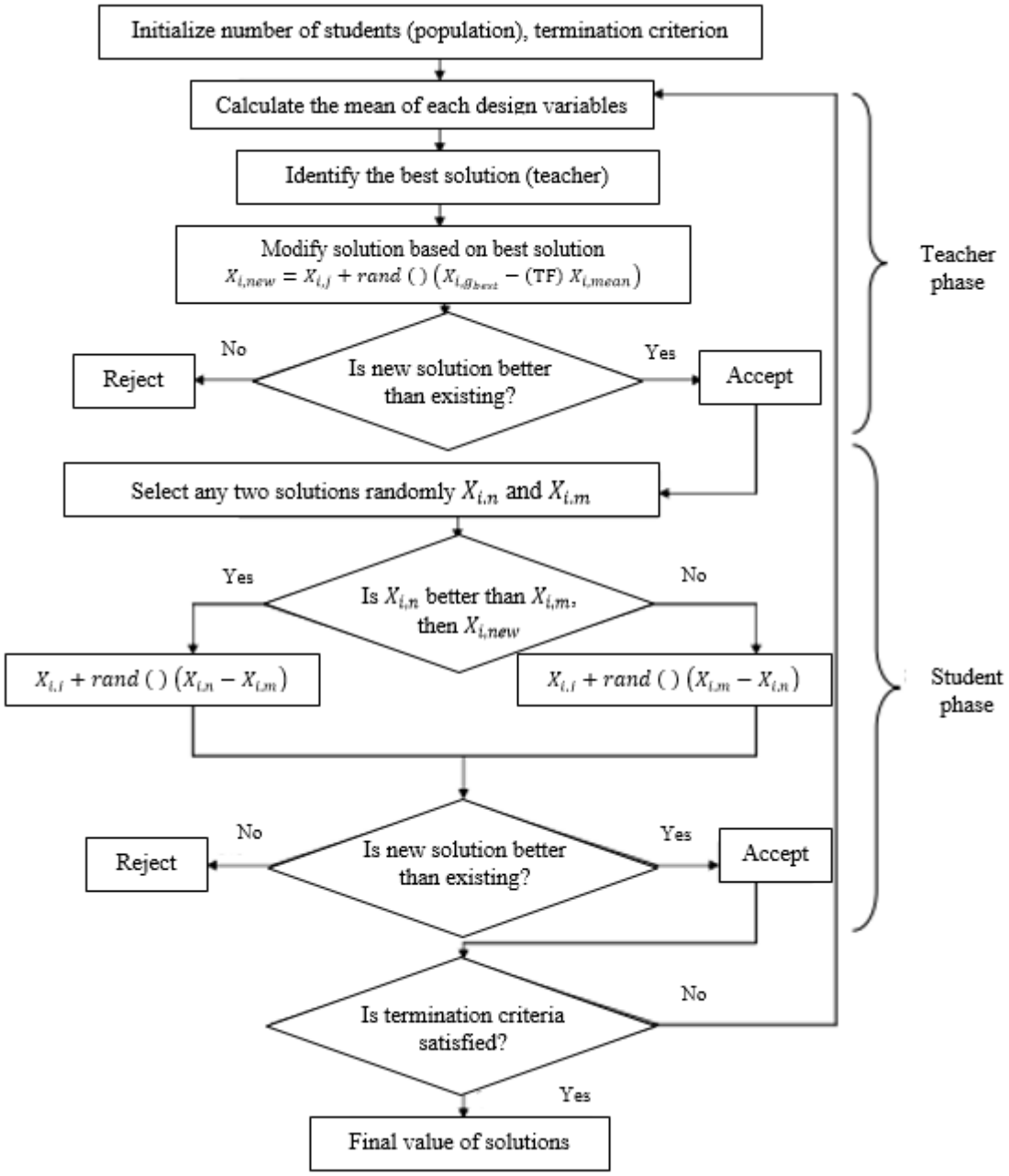

Fig. 2. The flowchart of TLBO (Rao et al., 2012).

5. Estimation Process via Multilayer Perceptrons (MLPs)

Multilayer perceptrons (MLPs) are one of the feed-forward artificial neural networks (ANNs) structure types that they have one input and one output layer together with one or more hidden layers. In these structures, there are many neurons, in other words, nodes taking place in these layers in the way of inspiration from neural cells within the natural mechanism of the human central neural system. In this sense, they perform to learn, analyze, solve problems, estimate, etc. by simulating the neural system and working system of it (Gardner and Dorling, 1998). In this respect, a decision-making model has developed thanks to the usage of different design combinations data, which were provided via optimization process by learned by MLPs that it takes place as "neural net fitting" within MATLAB R2018a program applications (MATLAB Mathworks). By this means, a speedy process for estimating optimal design properties

with the minimum total bar length becomes a possible application.

However, some of the design parameters, which are considered in the optimization process, will not be taken as constant in the machine learning operation applied for developing this decision-making model in the second step. In this way, a training set is generated via properties of optimum parameters belonging to various design combinations together with target function values corresponding to them, besides, Table 2 where the mentioned variable values are expressed, can be seen below.

Table 2. Properties of input ranges used for training.

Input parameters	Task	Ranges	Increment amount	Unit
P_1	Load applied on 1st node	95-100	0.25	kN
P_2	Load applied on 2nd node	45-50	0.25	kN
A	Section areas of truss bars	90-100	1	mm²

In here, loads as P_1 and P_2 with A are three inputs, and three outputs are optimum horizontal angles of bars (θ_1 and θ_2) and minimum total length of bars. It is stated that inputs and minimum bar length as objective function are adjusted in the range of [0, 0.6] by using a min-max normalization approach to be fitted and used in a similar range with other outputs (θ_1 and θ_2) (Eq. (15)) (Shamil, 2020). Where, $\bar{x}_i$ is the normalized value of ith data sample of any x attribute (x_i); $x_{\min}$ and $x_{\max}$ are biggest and smallest values within this attribute; $R_{\max}$ and $R_{\min}$ are limits defined as minimum and maximum, respectively, and they determine that normalization will be made in which ranges. Also, Fig. 3 shows the structure of the estimation model operated via MLPs.

$$\bar{x}_i = \left(\frac{x_i - x_{\min}}{x_{\max} - x_{\min}}\right)(R_{\max} - R_{\min}) + R_{\min} \quad (15)$$

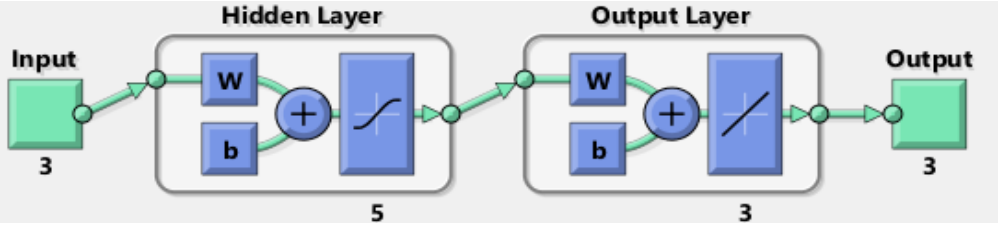

Fig. 3. Structure of decision-making model created for estimation of optimization data.

Furthermore, in the second step, a test and controlling dataset, which contains eight different optimum design combinations for a 5-bar truss structure, was generated to evaluate the principal learning model performance in terms of validation of test inputs and approximation to the target outputs. In this scope, for test combinations, some metrics (mean absolute error (MAE), mean squared error (MSE) and root mean squared error (RMSE)) were found for the errors, namely differences of test results according to real optimization outputs.

6. Numerical Examples

Correlation coefficients (R), which reflects the estimation and convergence success together with the degree of fitting between real values and predictions, were provided respect to training, validation, and test data, which belong to the main estimation model generated over dataset consisted from optimum results via TLBO, can be seen in Fig. 4. Also, error metrics are calculated as MAE, MSE and RMSE to observe the estimation performance of this model, and the results can be seen in Table 3.

As it can be seen from Fig. 4, all of the correlation results are pretty convenient, besides that each error rates are also extremely low in the meaning of successful convergence to real optimum results and validation of the model for design parameters and the normalized value of minimum total bar lengths (Table 3). In this regard, the model can be accepted as a usable tool and correct-estimator, and various new design data can be directly solved via this model to observe the desired optimum results without optimization processes. The generated test/controlling designs, and results of optimum parameters for them are given in Tables 4 and 5, respectively.

In Tables 6-8, concerning all test designs, MLPs estimations and errors for optimum parameter values and normalized minimum bar length were expressed with the aim of comparison via TLBO. Here, calculated metrics for error rates can be seen as MAE, MSE and RMSE.

Besides, estimations of normalized values of minimum total length of bars within Table 8, are benefited to figure out of actual values of the objective function as minimum bar length.

For this respect, normalizations are converted to real values as estimated data according to min-max normalization formulation, and detected results are evaluated by comparing them with optimum values (Table 9).

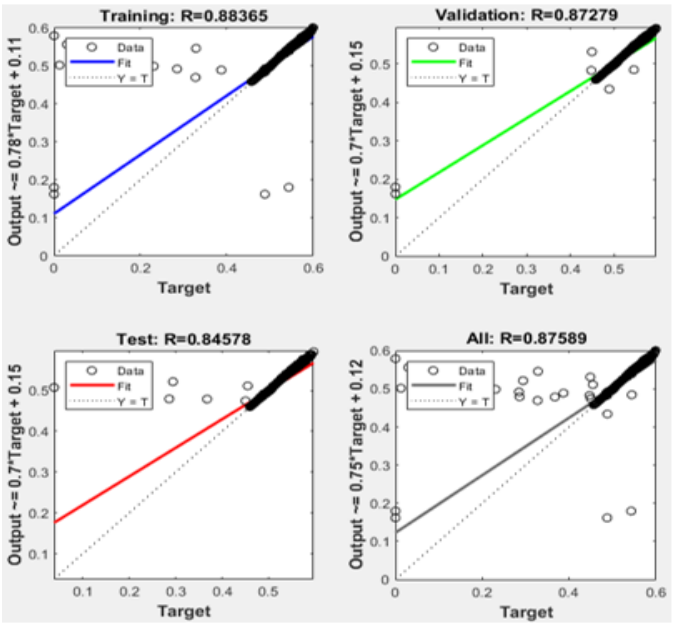

Fig. 4. Approximation and fitting performance of MLPs model for training, validation and testing data.

Table 3. Some evaluations for MLPs estimation model according to optimum results as training data.

Number of training sample for 5-bar truss	Error metrics		
	MAE	*MSE*	*RMSE*
θ_1 (rad)	1.24761e-03	1.95022e-04	1.39650e-02
θ_2 (rad)	1.24761e-03	1.95022e-04	1.39650e-02
Normalized (Min Total Length) (mm)	2.21334e-03	4.07848e-04	2.01952e-02

Table 4. Several combinations for test/controlling designs.

Cases for applied loads	Design number	Design parameters		
		P_1 (kN)	P_2 (kN)	A (mm²)
Between in defined limits	1	95.5	47.0	90.0
	2	100.0	49.25	100.2
	3	98.7	50.0	92.0
One of loads between in defined limits	4	95.8	52.0	91.3
	5	101.0	45.0	94.0
Except of defined limits	6	94.3	51.6	95.0
	7	102.6	44.5	92.5
	8	93.0	52.0	88.7

Table 5. Optimum values provided via TLBO for combinations of test designs.

Design number	TLBO results			Normalized (min total length) (mm)
	θ_1 (rad)	θ_2 (rad)	min $f(\theta_1.\theta_2)$: ΣL (mm)	
1	0.493203543	0.493203551	1135.3049	0.5560
2	0.474888911	0.474888922	1124.4249	0.5113
3	0.500114361	0.500114354	1139.5651	0.5735
4	0.500557327	0.500557337	1139.8412	0.5747
5	0.487223631	0.487223637	1131.6876	0.5412
6	0.483889577	0.483889577	1129.6983	0.5330
7	0.494758671	0.494758667	1136.2560	0.5599
8	0.503565683	0.503565688	1141.7252	0.5824

Table 6. Estimation results with errors of θ_1 compared with TLBO for each test design.

Design number	MLPs estimation	Errors according to TLBO	
	θ_1	Absolute error	Squared error
1	0.491908485	1.29506e-03	1.67717e-06
2	0.474715087	1.73824e-04	3.02148e-08
3	0.499395594	7.18767e-04	5.16626e-07
4	0.499640193	9.17134e-04	8.41135e-07
5	0.488572984	1.34935e-03	1.82075e-06
6	0.486492534	2.60296e-03	6.77539e-06
7	0.498448216	3.68954e-03	1.36127e-05
8	0.500770499	2.79518e-03	7.81306e-06
		MAE	MSE
	Mean	1.69273e-03	4.13589e-06
	RMSE		2.03369e-03

Table 7. Estimation results with errors of θ_2 compared with TLBO for each test design.

Design number	MLPs estimation	Errors according to TLBO	
	θ_2	Absolute error	Squared error
1	0.491908485	1.29507e-03	1.89391e-05
2	0.474715087	1.73834e-04	2.09410e-05
3	0.499395594	7.18759e-04	7.80162e-07
4	0.499640194	9.17144e-04	1.12704e-07
5	0.488572984	1.34935e-03	1.01318e-05
6	0.486492535	2.60296e-03	1.36866e-06
7	0.498448215	3.68955e-03	3.50331e-05
8	0.500770499	2.79519e-03	4.07105e-07
		MAE	MSE
	Mean	1.69273e-03	4.13589e-06
	RMSE		2.03369e-03

Table 8. Estimation results with errors of normalized values (min total length) compared with TLBO for each test design.

Design number	MLPs estimation	Errors according to TLBO	
	Normalized (min total length) (mm)	Absolute error	Squared error
1	0.491908485	1.29506e-03	1.67717e-06
2	0.474715087	1.73824e-04	3.02148e-08
3	0.499395594	7.18767e-04	5.16626e-07
4	0.499640193	9.17134e-04	8.41135e-07
5	0.488572984	1.34935e-03	1.82075e-06
6	0.486492534	2.60296e-03	6.77539e-06
7	0.498448216	3.68954e-03	1.36127e-05
8	0.500770499	2.79518e-03	7.81306e-06
		MAE	MSE
	Mean	1.69273e-03	4.13589e-06
	RMSE		2.03369e-03

Table 9. Converting the estimations of normalized values to actual results for minimum total bar length.

Design number	MLPs estimation	Errors according to TLBO	
	min $f(\theta_1.\theta_2)$: ΣL (mm)	Absolute error	Squared error
1	1134.6184	0.68649	0.47127
2	1124.4173	0.00758	0.00006
3	1139.2855	0.27961	0.07818
4	1139.2393	0.60190	0.36228
5	1132.8696	1.18197	1.39706
6	1131.3777	1.67941	2.82042
7	1139.4014	3.14534	9.89314
8	1139.8545	1.87075	3.49969
		MAE	MSE
	Mean	1.18163	2.31526
	RMSE		1.52160

7. Conclusions

In the present study, a hybrid application was conducted to determine numerical parameters for a structural engineering design problem as a truss model. In this respect, two independent phases were realized applied as metaheuristics-based optimization and machine learning estimation process, respectively. Here, for the first phase, optimum data for the training model was produced by utilizing a population-based optimization algorithm known as teaching-learning based optimization (TLBO); following, respect to the generation of a decision-making model, multilayer perceptrons (MLPs) were employed to estimate of defined outputs optimally, in the second phase.

For the current structural model as 5-bar, while considering of training and learning, estimation, and test processes of MLPs, this can be made as a comment that generated estimation model is very successful and capable in terms of estimating due to provided performance measurements such as correlation (almost R ≈ 88%), proper deviation and minimal errors (lower from 2% for all target outputs) among actual-predicted data. In this meaning, this model can be assumed as a predictor tool, and also benefited from converging to any parameter value of the presented structural model. Within this context, test and confirmation data were generated as different from training data which were produced intended for the usage of the establishment of the main estimation model only. According to the results of estimations and error rates, for test designs, it can be said that horizontal angles between bars and global axis (θ_1 and θ_2), and also minimum bar length (as normalized value) were determined with extremely small error amounts even if most test models' design parameters were considered as lower or upper levels from used input limits for training data.

On the other hand, the developed model is quite strong in the scope of foreseeing optimum values of best bar length, which was scaled/normalized to fit with other outputs, too. Here, it should be expressed that when estimated normalized values are transformed to target estimations for minimum bar length, definitely sufficient and remarkable error rates and so effectiveness arise according to actual optimization results for each test model. By this means, desired estimations for best bar lengths can be provided, too.

As a result, numerical estimation investigations were realized by using MPLs with the aim of detection process of objective parameters within any structural engineering design problem, and so a powerful, usable, and talented decision-making model was enhanced in terms of processing multiple data. Also, in future works, these methodologies can be evaluated for the different structural designs like reinforced concrete members, steel-frame models, slab systems, etc. To evaluate the optimization and machine learning technologies with a combination will be more valuable and usable for effective, optimal, and also cost and energy-effective solutions. Cause of these advantages, the mentioned and proposed methodology provides to decrease of the required effort, time and analysis steps besides that they make possible to precision measurements for the designs.

References

Brentan BM, Luvizotto Jr E, Herrera M, Izquierdo J, Pérez-García R (2017). Hybrid regression model for near real-time urban water demand forecasting. *Journal of Computational and Applied Mathematics*, 309, 532-541.

Cakiroglu C, Islam K, Bekdaş G, Billah M (2021). CO2 emission and cost optimization of concrete-filled steel tubular (cfst) columns using metaheuristic algorithms. *Sustainability*, 13(14), 8092.

Çerçevik AE, Avşar Ö, Hasançebi O (2020). Optimum design of seismic isolation systems using metaheuristic search methods. *Soil Dynamics and Earthquake Engineering*, 131, 106012.

Chakraborty D, Elhegazy H, Elzarka H, Gutierrez L (2020). A novel construction cost prediction model using hybrid natural and light gradient boosting. *Advanced Engineering Informatics*, 46, 101201.

Esfandiari MJ, Urgessa GS (2020). Progressive collapse design of reinforced concrete frames using structural optimization and machine learning. *Structures*, 28, 1252-1264.

Gardner MW, Dorling SR (1998). Artificial neural networks (the multilayer perceptron)—A review of applications in the atmospheric sciences. *Atmospheric Environment*, 32(14-15), 2627-2636.

Gholizadeh S, Mohammadi M (2017). Reliability-based seismic optimization of steel frames by metaheuristics and neural networks. *ASCE-ASME Journal of Risk and Uncertainty in Engineering Systems, Part A: Civil Engineering*, 3(1), 04016013.

Grossi E, Podda GM, Pugliano M, Gabba S, Verri A, Carpani G, Buscema M, Casazza G, Cattaneo M (2014). Prediction of optimal warfarin maintenance dose using advanced artificial neural networks. *Pharmacogenomics*, 15(1), 29-37.

Hosseinaei S, Ghasemi MR, Etedali S (2021). Optimal design of passive and active control systems in seismic-excited structures using a new modified TLBO. *Periodica Polytechnica Civil Engineering*, 65(1), 37-55.

Hu W, Xiao X, Xie D, Tan T, Maybank S (2004). Traffic accident prediction using 3-D model-based vehicle tracking. *IEEE Transactions on Vehicular Technology*, 53(3), 677-694.

Huang HC, Chang YL, Lan TH, Chiu HJ, Liu WM, Lee TJF (2008). Prediction of optimal lithium doses for Taiwanese psychiatric patients. *Journal of Clinical Pharmacy and Therapeutics*, 33(2), 115-121.

Huang C, Mezencev R, McDonald JF, Vannberg F (2017). Open source machine-learning algorithms for the prediction of optimal cancer drug therapies. *PLoS One*, 12(10), e0186906.

Kaveh A, Izadifard RA, Mottaghi L (2020). Optimal design of planar RC frames considering CO2 emissions using ECBO, EVPS and PSO metaheuristic algorithms. *Journal of Building Engineering*, 28, 101014.

Koo C, Hong T, Hyun C (2011). The development of a construction cost prediction model with improved prediction capacity using the advanced CBR approach. *Expert Systems with Applications*, 38(7), 8597-8606.

Lavasani SHH, Doroudi R (2020). Meta heuristic active and semi-active control systems of high-rise building. *International Journal of Structural Engineering*, 10(3), 232-253.

Lertpalangsunti N, Chan CW, Mason R, Tontiwachwuthikul P (1999). A toolset for construction of hybrid intelligent forecasting systems: Application for water demand prediction. *Artificial Intelligence in Engineering*, 13(1), 21-42.

Ly HB, Le TT, Vu HLT, Tran VQ, Le LM, Pham BT (2020). Computational hybrid machine learning based prediction of shear capacity for steel fiber reinforced concrete beams. *Sustainability*, 12(7), 2709.

Magdum SK, Adamuthe AC (2017). Construction cost prediction using neural networks. *ICTACT Journal on Soft Computing*, 8(1), 1549-1556.

Majid KI (1974). Optimum Design of Structures. Butterworth and Company Publishers Limited.

MATLAB (2018). Mathworks, Matlab 2018a. Neural Net Fitting. https://www.mathworks.com/ help/deeplearning/ref/neuralnetfitting-app.html.

McDonald JF, Mezencev R, Long TQ, Benigno B, Bonta I, Del Priore G (2015). Accurate prediction of optimal cancer drug therapies from molecular profiles by a machine-learning algorithm. *Journal of Clinical Oncology*, 33(15).

Moayyeri N, Gharehbaghi S, Plevris V (2019). Cost-based optimum design of reinforced concrete retaining walls considering different methods of bearing capacity computation. *Mathematics*, 7(12), 1232.

Msiza IS, Nelwamondo FV, Marwala T (2008). Water demand prediction using artificial neural networks and support vector regression. *Journal of Computers*, 3(11), 1.

Nigdeli SM, Bekdaş G (2019). Optimum design of multiple positioned tuned mass dampers for structures constrained with axial force capacity. *The Structural Design of Tall and Special Buildings*, 28(5), e1593.

Öztürk HT (2018). Cost optimum design of spread footing under uniaxial combined bending according to TS500 via various metaheuristic algorithms. *Pamukkale University Journal of Engineering Sciences*, 24(6), 1030-1036.

Rao R (2016). Review of applications of TLBO algorithm and a tutorial for beginners to solve the unconstrained and constrained optimization problems. *Decision Science Letters*, 5(1), 1-30.

Rao RV, Savsani VJ, Vakharia DP (2011). Teaching-learning-based optimization: a novel method for constrained mechanical design optimization problems. *Computer-Aided Design*, 43(3), 303-315.

Rao RV, Savsani VJ, Vakharia DP (2012). Teaching-learning-based optimization: an optimization method for continuous non-linear large scale problems. *Information Sciences*, 183(1), 1-15.

Shamil FR (2020). *Min max normalization in data mining*. https://t4tutorials.com/min-max-normalization-of-data-in-data-mining/. Downloaded on 27-08-2021.

Sharma S, Saha AK, Lohar G (2021). Optimization of weight and cost of cantilever retaining wall by a hybrid metaheuristic algorithm. *Engineering with Computers*, 1-27.

Shutian F, Tianyi Z, Ying Z (2017). Prediction of construction projects' costs based on fusion method. *Engineering Computations*, 34(7), 2396-2408.

Sikka S (2014). Prediction of road accidents in Delhi using back propagation neural network model. *International Journal of Computer Science & Engineering Technology* (*IJCSET*), 5(08).

Torkan M, Naderi Dehkordi M (2018). Development of ANFIS-PSO, SVR-PSO, and ANN- PSO hybrid intelligent models for predicting the compressive strength of concrete. *Iran University of Science & Technology*, 8(4), 547-563.

Ulusoy S, Kayabekir AE, Bekdaş G, Nigdeli SM (2018). Optimum design of reinforced concrete multi-story multi-span frame structures under static loads. *International Journal of Engineering and Technology*, 10(5), 403-407.

Ulusoy S, Kayabekir AE, Bekdaş G, Niğdeli SM (2020). Metaheuristic algorithms in optimum design of reinforced concrete beam by investigating strength of concrete. *Challenge Journal of Concrete Research Letters*, 11(2), 26-30.

Vellar LS, Ontiveros-Pérez SP, Miguel LFF, Fadel Miguel LF (2019). Robust optimum design of multiple tuned mass dampers for vibration control in buildings subjected to seismic excitation. *Shock and Vibration*.

Wenqi L, Dongyu L, Menghua Y (2017). A model of traffic accident prediction based on convolutional neural network. *2017 2nd IEEE International Conference on Intelligent Transportation Engineering* (*ICITE*), Singapore, 198-202.

Xia Z, Mao K, Wei S, Wang X, Fang Y, Yang S (2017). Application of genetic algorithm-support vector regression model to predict damping of cantilever beam with particle damper. *Journal of Low Frequency Noise, Vibration and Active Control*, 36(2), 138-147.

Yang L, Qi C, Lin X, Li J, Dong X (2019). Prediction of dynamic increase factor for steel fibre reinforced concrete using a hybrid artificial intelligence model. *Engineering Structures*, 189, 309-318.

Yaseen ZM, Tran MT, Kim S, Bakhshpoori T, Deo RC (2018). Shear strength prediction of steel fiber reinforced concrete beam using hybrid intelligence models: A new approach. *Engineering Structures*, 177, 244-255.

Yucel M, Bekdas G, Nigdeli SM, Sevgen S (2018). Artificial neural network model for optimum design of tubular columns. *International Journal of Theoretical and Applied Mechanics*, 3, 82-86.

Yücel M, Nigdeli SM, Bekdaş G (2020a). The comparison of classical and artificial neural network-based formulations for tuned mass damper optimization. *Proceedings of 6th International Conference on Harmony Search, Soft Computing and Applications* (*ICHSA 2020*), Istanbul, Turkey, 93-109.

Yücel M, Bekdaş G, Nigdeli, SM (2020b). Minimizing the weight of cantilever beam via metaheuristic methods by using different population-iteration combinations. *WSEAS Transactions on Computers*, 19, 69-77.

Yücel M, Nigdeli SM, Bekdaş G (2020c). Advances in Structural Engineering-Optimization. *In: Nigdeli SM, Bekdaş G, Kayabekir AE, Yucel M, editors. In Artificial Intelligence and Machine Learning with Reflection for Structural Engineering: A Review*. Springer, 23-72.

Zhang J, Huang Y, Wang Y, Ma G (2020). Multi-objective optimization of concrete mixture proportions using machine learning and metaheuristic algorithms. *Construction and Building Materials*, 253, 119208.

Zubaidi SL, Ortega-Martorell S, Al-Bugharbee H, Olier I, Hashim KS, Gharghan SK, Kot P, Al-Khaddar R (2020). Urban water demand prediction for a city that suffers from climate change and population growth: Gauteng province case study. *Water*, 12(7), 1885.

Challenge Journal of Structural Mechanics

Research Article

Optimization of cylindrical wall domes via metaheuristic algorithms

Aylin Ece Kayabekir [a,*]

[a] *Department of Civil Enginering, İstanbul Gelişim University, 34310 İstanbul, Turkey*

ABSTRACT

Optimization is a widely used phenomenon in various problems and fields. Because time and resources are very limited in today's world, it can be said that the usage area of the optimization process will be expanded and spread in all areas of life. Although different methods are used in the realization of the optimization process, the performance of metaheuristic algorithms in solving problems has led to an increase in research on these methods. As in other fields, the application examples of these algorithms are diversifying and increasing in the field of structural engineering. In this study, the performance comparison of five different algorithms for the optimum design of an axisymmetric cylindrical wall with a dome is investigated. These algorithms are Jaya (JA), Flower pollination (FPA), teaching-learning-based optimization (TLBO) algorithms and two hybrid versions of these algorithms. ACI 318 regulation was used in reinforced concrete design with a flexibility method-based approach in the analyses. In the analyzes with five different situations of the wall height, some statistical values , and data of analysis numbers were obtained by running the algorithms a large number of times. According to the analysis results, Jaya algorithm is slightly better in terms of the speed of reaching the optimum result, but also all algorithms are quite effective and reliable in solving the problem.

ARTICLE INFO

Article history:
Received 3 October 2021
Revised 1 November 2021
Accepted 29 November 2021

Keywords:
Metaheuristic algorithms
Hybrid algorithm
Flower pollination
Teaching-learning based optimization
Cylindrical walls
Reinforced concrete design

1. Introduction

In almost all of the natural events that take place in the world, it is seen that the events operate in the most appropriate order under various conditions such as time, situation, and environmental conditions, and the operation is updated to maintain the most appropriate order in the face of changing situations.

These events, which take place for various reasons such as migration, hunting, movement in a hierarchical order, usually take place to survive in the balance of nature. For this reason, the process must be in the most appropriate way according to environmental factors. The most appropriate order seen in the behavior of other living things can be observed in the design and processes of civilizations established by humans, such as the locations of cities, road routes, tools used, city infrastructure systems, structural designs, defense systems. However, the main difference between humans and other living things is that while other creatures manage the processes with their intuition, people's intuitions and their minds, which include various processes such as observation, experience, and thinking, evaluate the situation and act. Today, many engineering designs have been developed as a result of these observations of nature by scientists, and have been presented to humanity in many different ways, directly or indirectly. Metaheuristic algorithms can be given as an example of this situation.

Metaheuristic algorithms are methods developed as a result of mathematical equations expressing the heuristic behaviors of living things to maintain processes such as movement, migration, feeding in the most appropriate way possible as a result of nature observations, and are generally used for optimization purposes. Examples of metaheuristic algorithms, the variety and number of which have increased with the development of computer processor technology, are presented in Table 1.

* *Corresponding author*. E-mail address: aekayabekir@gelisim.edu.tr (A. E. Kayabekir)
ISSN: 2149-8024 / DOI: https://doi.org/10.20528/cjsmec.2021.04.003

Table 1. Metaheuristic algorithms and origins.

Name	Developer	Observation
Genetic Algorithm	Holland (1975)	Nature evolutionary mechanisms
Simulated Annealing	Kirkpatrick et al. (1983)	Metal heating-cooling process
Particle Swarm Optimization	Kennedy and Ebarhart (1995)	Social behavior during the movement of organisms
Differential Evaluation	Storn and Price (1997)	Evolutionary process
Harmony Search	Geem et al. (2001)	Musical processes
Big bang-big Crunch	Erol and Eksin (2006)	Big-bang big-crunch theory of universe evolution
Artificial Bee Colony Algorithm (ABC)	Karaboga and Basturk (2007)	Foraging intelligence of bee
Cuckoo Search Algorithm	Yang and Deb (2009)	The parasitic process in the cuckoo brood
Firefly Algorithm	Yang (2009)	Flashing light behavior of fireflies
Bat Algorithm	Yang (2010)	Bats echolocation behaviour used for search directions and location
Teaching-learning based Optimization	Rao et al. (2011)	Teacher and learner roles during education
Flower Pollination Algorithm	Yang (2012)	Pollination process of flowers
Krill Herd	Gandomi and Alavi (2012)	Herding behavior of krill's
Grey Wolf Optimizer	Mirjalili et al. (2014)	The hierarchy between grey wolf packs
Jaya Algorithm	Rao (2016)	Victory means in Sanskrit

Today, metaheuristic algorithms of optimization problems are frequently used in many engineering fields. One of them is the field of structural engineering, which is one of the sub-branches of civil engineering, where studies are carried out within the scope of structural design. Examples of optimization problems in which metaheuristic algorithms are used in structural engineering are beams (Coello et al., 1997; Rafiq and Southcombe, 1998; Govindaraj and Ramasamy, 2005; Akın and Saka, 2010; Fedghouche and Tiliouine, 2012; Bekdaş and Nigdeli, 2013; Kayabekir et al., 2019; Zhao et al., 2021), columns (Bekdaş and Nigdeli, 2014; 2016a; 2016b; de Medeiros and Kripta, 2014; Nigdeli et al., 2015; Cakiroglu et al., 2021), frames (Bekdaş and Nigdeli, 2017; Nigdeli and Bekdaş, 2016; Ghatte, 2021), foundations (Nigdeli et al., 2018; Kashani et al., 2021), retaining walls (Ceranic et al., 2001; Yepes et al., 2008; Camp and Akin, 2011; Kayabekir et al., 2020; Yücel et al., 2021; Martínez-Muñoz et al., 2021; Shalchi Tousi et al., 2021), Carbon Fiber Reinforced Polymer retrofit (Kayabekir et al., 2017; 2018) and cylindrical walls (Bekdaş, 2014; 2015; 2018; 2019; Kayabekir, 2021).

In this study, the optimum design of axially symmetrical cylindrical reinforced concrete walls with a dome on top has been investigated. In the optimization problem, the objective function is defined as the minimization of the total cost of the cylindrical wall consisting of steel and concrete. Long cylindrical walls were assumed in the analyzes and the flexibility method was used to calculate the internal forces. Hybrid algorithms of Flower Pollination Algorithm, Jaya Algorithm and Teaching Learning-Based Optimization have been proposed for optimization. The performance of the hybrid algorithm was tested under various conditions of the cylindrical wall. Then, these analysis results were also compared with the Flower pollination algorithm, teaching learning-based algorithm, and Jaya, which are known to be effective in the literature in optimization.

2. Optimum Design Methodology

In this section, the methodology including the details of the application of metaheuristic algorithms to the optimization problem is presented. In the literature, in optimization problems in which metaheuristic algorithms are used in general, the methodology is collected in five main steps. The operations performed in steps 1, 2, 3, and 5 of these five steps are similar in almost all algorithms. Only the operation performed in step 4 includes some algorithm-specific mathematical expressions. These five steps and the operations performed in each step are summarized below.

In the first step, the data entry of the problem is done. These data are design constants, ranges of design variables and special parameters of the optimization algorithm, number of solution vectors (*vn*), and stopping criteria (*sc*). Information about the design constants and design variables used in optimization are given in Tables 2 and 3, respectively.

Some of the algorithms, especially those developed in recent years, are parameter-free, that is, they do not have algorithm-specific parameters. Except for FPA, this study is parameter-free in the algorithms used. FPA algorithm has a parameter called switch probability (*sp*).

The stopping criterion, which stops the optimization process, is used in different ways in the literature. One of these, perhaps the most common, is to set a maximum value for iterations. This approach was also applied in this study. In this study, *vn*, *sp*, and *sc* values were taken as 20, 0.5, and 20000, respectively.

Table 2. The design constants of the optimization problem.

Description	Symbol	Unit	Value
Radius of wall	R	m	18
Height of the wall	H	m	5-7
Height of the dome	H_d	m	3
The thickness of the dome	h_d	m	0.25
Yield strength of steel	f_y	MPa	420
Concrete cover	c_c	mm	50
Compressive strength of concrete	f'_c	MPa	30
The elasticity modulus of concrete	E_c	MPa	$4700(f'_c)^{1/2}$
Poisson ratio of concrete	ν	-	0.2
Density of liquid	γ	kN/m^3	10
Minimum reinforcement ratio	ρ_{min}	-	0.008
Unit concrete cost	Cc	TL/m^3	290
Unit steel cost	Cs	TL/ton	7400

Table 3. The design variables and ranges of the optimization problem.

Description	Symbol	Unit	Range
The thickness of the wall	hw	m	0.2-2.0
Diameter of the steel bars	R	mm	8-60
Spacing between the steel bars	S	mm	$S_{min}^{*} \le S_h \le S_{max}^{\#}$

$^{*}S_{min}=\max(25, \phi)$ and $^{\#}S_{max}=\max(450, 5h_w)$

In the second step, the initial solution matrix is constructed. This matrix contains randomly generated design variables within the range for each solution vector (Table 3). Each design variable is generated between the lower and upper limits as in Eq. (1) and stored in the corresponding row of the solution vector.

$$X_i = X_{i(\min)} + \text{rand}(X_{i(\max)} - X_{i(\min)}) \quad (1)$$

In the equation, $X_{i\,(\min)}$ and $X_{i\,(\max)}$ represent the lower and upper limits of the i^{th} design variable, respectively, and the rand is a function that produces a single uniformly distributed random number in the interval (0,1).

The third step includes the analysis and design phases. In this step, analysis and design are done for each solution vector, and then the objective function is calculated. In this study, the sum of the steel and concrete costs of the cylindrical wall design is defined as the objective function (Eq. (2)).

$$f(x) = C_c V_c + C_s W_s \quad (2)$$

In the equation, V_c and W_s represent the total concrete volume and steel weight, respectively.

Analyzes were done using the flexibility theory (see in Section 3) according to the assumption of a long cylindrical wall, and the design was done by the requirements of ACI 318-Building code requirements for structural concrete. Accordingly, the constraints controlled during the design process are presented in Table 4.

Table 4. The design constraints of the optimization problem.

Description	Symbol
Flexural strength capacity, M_d	$M_d \ge M_u$
Shear strength capacity, V_d	$V_d \ge V_u$
Minimum steel ratio, $\rho_{\min}$	$A_s \ge A_{s\min}$
Maximum steel bars spacing, $S_{\max}$	$S \le S_{\max}$
Minimum steel bars spacing, $S_{\min}$	$S \ge S_{\min}$
Minimum concrete cover, $c_{c\min}$	$c_{c\min} \ge 40$ mm

If these constraints are not satisfied in any solution vector, the process called punishment is applied. It is known that there are different types of punishment in the literature. In this study, punishment is done by equating the objective function to a very large value.

Since the target in optimization is to obtain the lowest cost design, this penalty in the objective functions ensures that these solutions are eliminated in the following steps, thus convergence to the lowest solutions. In the study, this penalty value was taken as 10^6.

The fourth step is the step in which new solution vectors are obtained according to the algorithm rules. As mentioned before, this step is unique in algorithms because each algorithm applies its own rules.

In this study, JA, TLBO, FPA, and two hybrid algorithms were applied to the problem and the performances of the algorithms were compared. These algorithms were proved as effective ones in structural engineering problems and include unique features. The use

of Levy distribution, being a user-defined specific parameter-free algorithm and being a single-phase method using both of best and worst solutions in an equation are the unique features of FPA, TLBO and JA, respectively. These unique features provide differentiation of these algorithms. To reach a better solution sensitively, the classical algorithms need to be improved and hybrid algorithms are constructed via these algorithms. The equations used to generate a new solution matrix for these algorithms are given below.

The Jaya algorithm is a parameter-free algorithm using a single equation. In the algorithm, each solution (for example $X^t_{i,j}$ is the i^{th} solution) is tried to be improved by using the best (g^*) and worst (g^w) solutions in terms of the objective function. Accordingly, a new solution ($X^{t+1}_{i,j}$) can be found as follows

$$X^{t+1}_{i,j} = X^t_{i,j} + \text{rand}(g^* - X^t_{i,j}) - \text{rand}(g^w - X^t_{i,j}) \quad (3)$$

In the TLBO algorithm, two different equations such as FPA are used in new solutions. These are called the teacher and student phases, respectively. However, unlike the choice done depending on the *sp* value in FPA, these two equations are applied sequentially in TLBO.

The teacher role is the person who has the best knowledge in the classroom and teaches the others. In the teacher phase of the algorithm, this corresponds to the solution with the best objective function among the solution vectors. According to this, the teacher phase can be written as

$$X^{t+1}_{i,j} = X^t_{i,j} + \text{rand}\left(g^* - TF\ X^t_{\text{mean},j}\right) \quad (4)$$

In this equation, $X^t_{\text{mean},j}$ is the mean value of the design variables, and TF, called the teaching factor, is a coefficient calculated according to Eq. (5).

$$TF = \text{round}\left(1 + \text{rand}\,(\,)\right) \quad (5)$$

The student phase, on the other hand, stimulates the learning of students as a result of their interaction. This situation, which shows the interaction of randomly selected solutions ($X^t_{m,j}$ and $X^t_{n,j}$) is seen in Eq. (6).

$$X^{t+1}_{i,j} = \begin{cases} f(X)_n < f(X)_m, & X^t_{i,j} + \text{rand}(X^t_{m,j} - X^t_{n,j}) \\ f(X)_n > f(X)_m, & X^t_{i,j} + \text{rand}(X^t_{n,j} - X^t_{m,j}) \end{cases} \quad (6)$$

According to the FPA, new solutions can be produced according to two different equations. These equations simulate global and local pollination, respectively. The equation to be used in generating a new value is decided according to the switch probability (*sp*) value. Accordingly, a random value is generated with the rand function and compared with *sp*. If the rand value is less than *sp*, global pollination is applied (Eq. (7)), otherwise, local pollination is applied (Eq. (8)). Levy flight, which is the value simulating the flight of pollen in the global pollination equation, is defined by the letter *L*.

$$X^{t+1}_{i,j} = X^t_{i,j} + L(g^* - X^t_{i,j}) \quad (7)$$

$$X^{t+1}_{i,j} = X^t_{i,j} + \text{rand}(X^t_{m,j} - X^t_{n,j}) \quad (8)$$

The hybrid algorithms used in the study consist of the student phase/local pollination phase with Jaya. In addition, a modification was done to the Jaya equation by using *L* instead of the rand function as given in Eq. (9).

$$X^{t+1}_{i,j} = X^t_{i,j} + L(g^* - X^t_{i,j}) - L(g^w - X^t_{i,j}) \quad (9)$$

During the optimization, for the first hybrid algorithm called JALS, one of the Eq. (8) and Eq. (9) is used to generate new solutions according to the switch probability value defined in FPA.

The second hybrid algorithm, JALS2 is used two phases consecutively like TLBO. In these phases, both Eq. (8) and Eq. (9) in the generation of new solutions. In these phases, the production of new solutions is done according to Eq. (8) and Eq. (9), respectively.

In the last step, new solutions are compared with existing solutions. If objective function value of new solutions better than existing ones, existing solution matrix is updated with new solutions. Otherwise no change is done. The last step and the fourth step are continued as satisfied stopping criteria of the optimization. The optimization process defined in five steps is also summarized with the pseudo code in Fig. 1.

Step 1: Data entering process
Enter design constants (Table 2), ultimate limit of design variables (Table 3), algorithm parameters, number of solution vectors (vn) and stopping criteria (sc).

Step 2: Initial solution matrix generation process
Generate total vn solution vectors according to Eq. (1), including randomly generated design variables and save the vectors in the initial solution matrix.

Step 3: Analysis and design process
Analyze and design the system using each solution vector. Then, calculate the objective function (Eq. (2)) for each solution vector and stored in the objective function vector.

while *iteration number <stopping criteria (sc)*

Step 4: Initial solution matrix generation process
Generate new solution vectors according to the algorithm rules.

Step 5: Comparing of solution matrices
if *objective function value of new solutions better than existing ones*
Modify the existing solution matrix
end *(if)*

end *(while)*

Fig. 1. Pseudo code of optimization process.

3. Analysis of Axially Symmetrical Cylindrical Shells

A small piece of the shell shown in Fig. 2 can be taken to obtain the general solution for cylindrical shells. Considering the equilibrium condition by taking into account symmetry and some constant forces, Eq. (10) can be written.

$$\frac{dN_x}{dx} r dx d\varphi = 0$$

$$\frac{dQ_x}{dx} r dx d\varphi + N_\varphi dx d\varphi + q r dx d\varphi = 0$$

$$\frac{dM_x}{dx} r dx d\varphi - Q_x r dx d\varphi = 0 \quad (10)$$

From the solution of these equations to the axially symmetrical cylindrical shell conditions with appropriate assumptions, the general solution can be defined as

$$w = e^{\beta x}(C_1 \cos\beta x + C_2 \sin\beta x) + e^{-\beta x}(C_3 \cos\beta x + C_4 \sin\beta x) + f(x) \quad (11)$$

where $C_{1\text{-}4}$ are integration constants that depend on support conditions, $f(x)$ is a particular solution. β is a notation used in differential equation solutions and is given in Eq. (12).

$$\beta^4 = \frac{Eh}{4r^2 D} = \frac{3(1-\nu^2)}{r^2 h^2} \quad (12)$$

In the equation, E, h, r, D, and ν are elasticity modulus, thickness, radius, rigidity (Eq. (13)), and Poisson's ratio, respectively.

$$D = \frac{Eh^3}{12-(1-\nu^2)} \quad (13)$$

When the structure of this equation is examined, it is seen that the effects on the wall decrease rapidly as you move away from the point where the load affects, and converge to zero after a certain point. In this case, it means that the cylindrical wall of a certain length and the wall of infinite length give approximately the same results. This approach greatly simplifies the general equation whose solution includes assumptions and complex mathematical operations. The solution equation of this situation, which is called the long wall, can be written as

$$w = e^{-\beta x}\,(C_3 \cos\beta x + C_4 \sin\beta x) \quad (14)$$

Detailed information about this situation can be found in several books (Billington, 1965; Timoshenko and Woinowsky-Krieger, 1984).

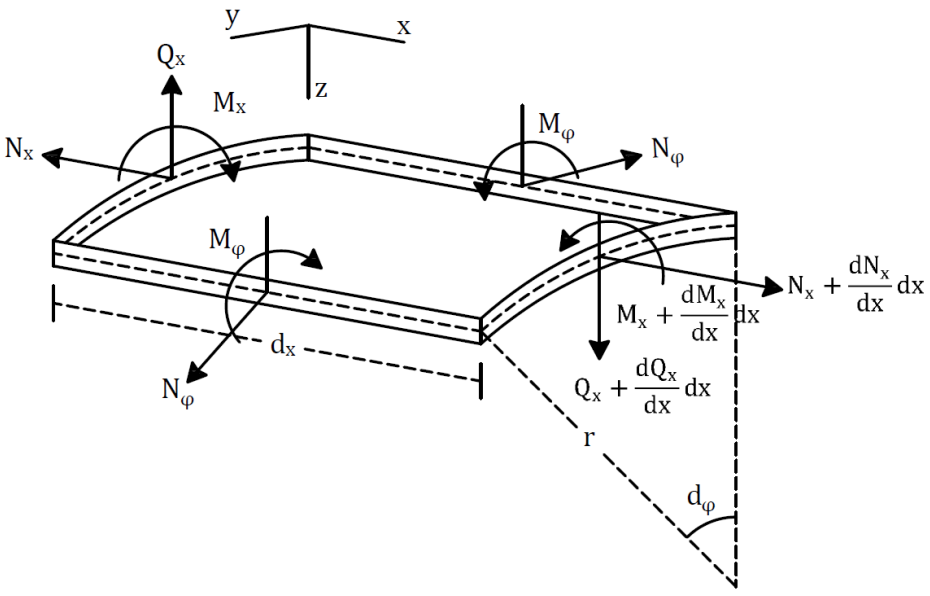

Fig. 2. A small element of circular cylindrical shell.

4. Analysis of Cylindrical Wall with Flexibility Theory

In Fig. 3, a cylindrical wall under the water loading with a fixed base supported and the unknown forces in the equivalent isostatic system can be seen.

The compatibility equations for the structure can be written as

$$D_{10} + F_{11}X_1 + F_{12}X_2 = 0$$

$$D_{20} + F_{22}X_2 + F_{21}X_2 = 0 \quad (15)$$

In the equation, D_{10}, D_{20} are displacement terms; F_{11}, F_{12}, F_{21}, and F_{22} are flexibility coefficients. The equations of these terms are as follows

$$D_{10} = -\frac{\gamma r^2 H}{Eh} \quad and \quad D_{20} = \frac{\gamma r^2}{Eh} \quad (16)$$

$$F_{11} = \frac{1}{2\beta^3 D}\ ,\ F_{22} = \frac{1}{\beta D} \quad and \quad F_{12} = F_{21} = -\frac{1}{2\beta^2 D} \quad (17)$$

where γ is liquid density and H is height of the wall. By implementing Eqs. (16-17) to Eq. (15), redundant forces can be obtained as

$$\begin{bmatrix} X_1 \\ X_2 \end{bmatrix} = F^{-1} \begin{bmatrix} -\frac{\gamma \cdot r^2 \cdot H}{E \cdot h} \\ \frac{\gamma \cdot r^2}{E \cdot h} \end{bmatrix} \quad (18)$$

These two forces are those that only occur in the case of a cylindrical wall. In the case of a dome on the wall, the displacement (Eq. (19)) and flexibility (Eq. (20)) terms of the dome can be added to the wall terms and the result can be obtained easily.

$$D_{10d} = \frac{r_d^2 q}{E_d h_d}\left(\frac{1+\nu_d}{1+\cos\alpha} - \cos\alpha\right)\sin\alpha$$

$$D_{20d} = \frac{r_d q}{E_d h_d}(2 + \nu_d)\sin\alpha \quad (19)$$

$$F_{11d} = \frac{2 r_d \lambda_d \sin^2\alpha}{E_d h_d} \quad , \quad F_{12d} = F_{21d} = \frac{2\lambda_d^2 \sin\alpha}{E_d h_d} \quad ,$$

$$\text{and} \quad F_{22d} = \frac{4\lambda_d^3}{E_d h_d r_d} \quad (20)$$

In these equations, r_d, ν_d, α, E_d, λ_d, and h_d are radius, Poisson's ratio, starting angle, elasticity modulus, a term that contains several properties of dome and thickness of the dome, respectively. After the values in the equation are calculated and added to the wall terms (F_s, D_{10s} and D_{20s}), the unknown forces at the top of the wall can be calculated as

$$\begin{bmatrix} X_3 \\ X_4 \end{bmatrix} = F_s^{-1} \begin{bmatrix} D_{10s} \\ D_{20s} \end{bmatrix} \quad (21)$$

A further explanation for this application can be found in Billington (1965) and Kayabekir (2021).

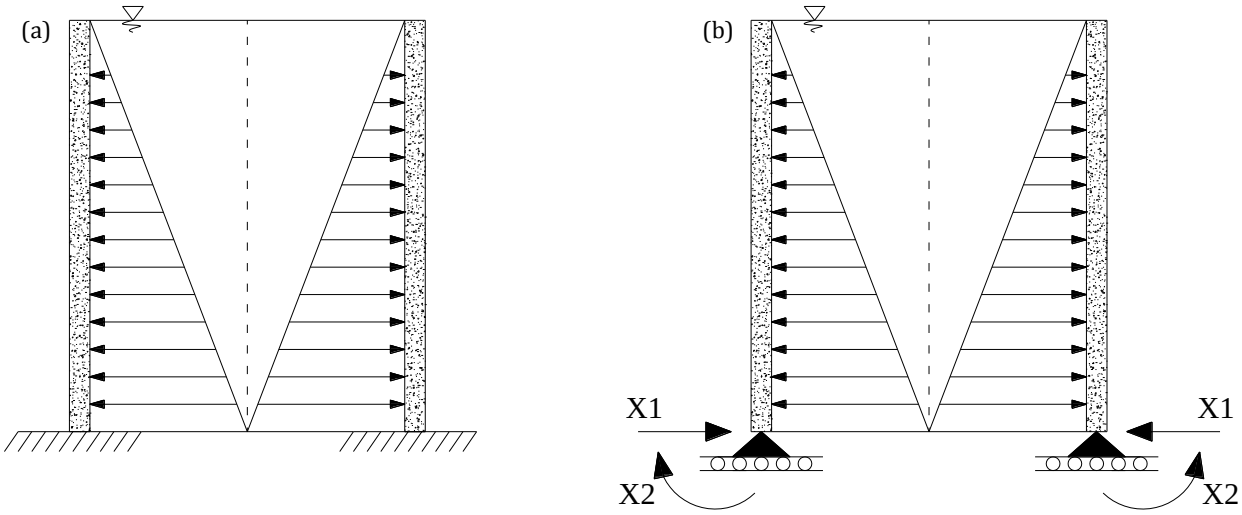

Fig. 3. a) A Fixed based wall; b) Equivalent statically determinate system.

5. Numerical Examples

In this section, optimization via metaheuristic-based optimization methodologies JA, JALS, JALS2, FPA, and TLBO are performed for 5 cases including different wall heights, from 5m to 7m with 0.5m increments. The optimization process of each case was done for 20 runs.

The optimum thickness of the wall (*hw*) and statistical values of the objective function are given in Table 5. Table "Min. cost", "Ave. cost", "SD" and "Analyses num." show minimum cost, average cost, standard deviation, and the average analysis number for which the optimum result is found respectively.

It can be seen from Table 5 that the optimum wall thickness increases as the wall height increases. Therefore, as the height increases, the cost also increases. This increase between two consecutive cases was approximately 12.43% - 16.28% for *hw* and 21.88% - 26.85% for minimum cost. In addition, as the wall height increases, the differences between successive cases decrease.

Considering the *hw* and minimum cost values calculated for each case, it is seen that the algorithms find approximately the same results.

According to statistical data, the standard deviation value for each algorithm is very close to zero. This situation shows that the algorithms find the nearly same minimum cost value in each run for a cylindrical wall problem having one design variable, that is, the algorithms provide stable results. For that reason, the average cost values are also similar.

Although the algorithms provide similar results, they reach optimum results at different analysis numbers. For all cases, JA reaches the optimum result very quickly with a 56.2-58.4 average analysis number. Hybrid algorithms, JALS (analyses number 177.45-206.2) and JALS2 (analyses number 178.3-201.3) have similar performance with FPA (analyses number 179.15-197.1). TLBO shows the lowest performance with 322.4-367 analyses number.

Table 5. Optimum results for 5 cases.

Cases	Results	JA	JALS	JALS2	FPA	TLBO
Case 1 (*H*=5m)	*hw* (m)	0.4747	0.4747	0.4747	0.4747	0.4747
	Min. cost (TL)	131082.69	131082.69	131082.69	131082.69	131082.69
	Ave. cost (TL)	131082.69	131082.69	131082.69	131082.69	131082.69
	SD (TL)	3E-11	3E-11	3E-11	3E-11	3E-11
	Analyses num.	56.2	188.45	190	191.7	344.3
Case 2 (*H*=5.5m)	*hw* (m)	0.5520	0.5520	0.5520	0.5520	0.5520
	Min. cost (TL)	166280.09	166280.09	166280.09	166280.09	166280.09
	Ave. cost (TL)	166280.09	166280.09	166280.09	166280.09	166280.09
	SD (TL)	3E-11	3E-11	3E-11	3E-11	3E-11
	Analyses num.	56.2	190.4	192.4	185.85	355
Case 3 (*H*=6m)	*hw* (m)	0.6346	0.6346	0.6346	0.6346	0.6346
	Min. cost (TL)	207784.58	207784.58	207784.58	207784.58	207784.58
	Ave. cost (TL)	207784.58	207784.58	207784.58	207784.58	207784.58
	SD (TL)	3E-11	3E-11	3E-11	3E-11	3E-11
	Analyses num.	56.85	177.45	178.3	179.15	322.4
Case 4 (*H*=6.5m)	*hw* (m)	0.7188	0.7188	0.7188	0.7188	0.7188
	Min. cost (TL)	254704.58	254704.58	254704.58	254704.58	254704.58
	Ave. cost (TL)	254704.58	254704.58	254704.58	254704.58	254704.58
	SD (TL)	4E-10	3E-11	3E-11	3E-11	3E-11
	Analyses num.	58.4	206.2	196.2	197.1	367
Case 5 (*H*=7m)	*hw* (m)	0.8082	0.8082	0.8082	0.8082	0.8082
	Min. cost (TL)	310424.16	310424.16	310424.16	310424.16	310424.16
	Ave. cost (TL)	310424.16	310424.16	310424.16	310424.16	310424.16
	SD (TL)	3E-10	1E-10	1E-10	1E-10	1E-10
	Analyses num.	57.55	192.4	201.3	193.35	350.8

6. Conclusions

In the present study, the performances of several classical and hybrid metaheuristic algorithms are compared on the optimum design of axially symmetrical cylindrical reinforced concrete walls with a dome on top. In the analysis, five different situations, three of which are classical and two of which are hybrid, of five different algorithms and different wall heights were examined. Algorithm performances were compared in terms of minimum, average, standard deviation values , and the number of analyzes in which optimum results were achieved by running the algorithms in large numbers for each case.

According to the analysis results, it is understood that all algorithms reach the optimum result. In addition, it is seen from the mean and standard deviation values of the repeated run results that the algorithms successfully perform the optimization process each time. According to these data, it can be said that all algorithms are used to give reliable and appropriate results for the optimization problem.

According to another comparison parameter, the number of analysis values, it is seen that the Jaya algorithm is the fastest in all cases. In addition, it is understood that the slowest algorithm is TLBO, although other algorithms are close to each other, the JALS algorithm is slightly faster in 3 out of 5 cases. These results show that the use of the Jaya equation for both the global equation of the FPA algorithm and the teacher phase of the TLBO algorithm contributes to the improvement of the performance of both algorithms.

In future studies, it will be useful to demonstrate the effectiveness of the methods by researching with a variety of problem and design variants.

References

Akin A, Saka MP (2010). Optimum detailed design of reinforced concrete continuous beams using the Harmony Search Algorithm. *Tenth International Conference on Computational Structures Technology*, Stirlingshire, UK, 131.

Bekdas G (2014). Optimum design of axially symmetric cylindrical reinforced concrete walls. *Structural Engineering and Mechanics*, 51(3), 361-375.

Bekdaş G (2015). Harmony Search Algorithm approach for optimum design of post-tensioned axially symmetric cylindrical reinforced concrete walls. *Journal of Optimization Theory and Applications*, 164(1), 342-358.

Bekdaş G (2018). New improved metaheuristic approaches for optimum design of posttensioned axially symmetric cylindrical reinforced concrete walls. *The Structural Design of Tall and Special Buildings*, 27(7), e1461.

Bekdaş G (2019). Optimum design of post-tensioned axially symmetric cylindrical walls using novel hybrid metaheuristic methods. *The Structural Design of Tall and Special Buildings*, 28(1), e1550.

Bekdaş G, Nigdeli SM (2013). Optimization of T-shaped RC flexural members for different compressive strengths of concrete. *International Journal of Mechanics*, 7, 109-119.

Bekdas G, Nigdeli SM (2014). The optimization of slender reinforced concrete columns. *PAMM*, 14(1), 183-184.

Bekdas G, Nigdeli SM (2016a). Bat algorithm for optimization of reinforced concrete columns. *PAMM*, 16(1), 681-682.

Bekdaş G, Nigdeli SM (2016b). Optimum design of reinforced concrete columns employing teaching learning based optimization. *12th International Congress on Advances in Civil Engineering*, 1-8.

Bekdaş G, Nigdeli SM (2017). Modified harmony search for optimization of reinforced concrete frames. *International Conference on Harmony Search Algorithm*, Springer, Singapore, 213-221.

Billington DP (1965). Thin Shell Structures. McGraw-Hill, New York.

Cakiroglu C, Islam K, Bekdaş G, Billah M (2021). CO_2 emission and cost optimization of concrete-filled steel tubular (CFST) columns using metaheuristic algorithms. *Sustainability*, 13(14), 8092.

Camp CV, Akin A (2011). Design of retaining walls using big bang–big crunch optimization. *Journal of Structural Engineering*, 138(3), 438-448.

Ceranic B, Fryer C, Baines RW (2001). An application of simulated annealing to the optimum design of reinforced concrete retaining structures. *Computers & Structures*, 79(17), 1569-1581.

Coello CC, Hernández FS, Farrera FA (1997). Optimal design of reinforced concrete beams using genetic algorithms. *Expert systems with Applications*, 12(1), 101-108.

de Medeiros GF, Kripka M (2014). Optimization of reinforced concrete columns according to different environmental impact assessment parameters. *Engineering Structures*, 59, 185-194.

Erol OK, Eksin I (2006). A new optimization method: big bang–big crunch. *Advances in Engineering Software*, 37(2), 106-111.

Fedghouche F, Tiliouine B (2012). Minimum cost design of reinforced concrete T-beams at ultimate loads using Eurocode2. *Engineering Structures*, 42, 43-50.

Gandomi AH, Alavi AH (2012). Krill herd: a new bio-inspired optimization algorithm. *Communications in Nonlinear Science and Numerical Simulation*, 17(12), 4831-4845.

Geem ZW, Kim JH, Loganathan GV (2001). A new heuristic optimization algorithm: harmony search. *Simulation*, 76(2), 60-68.

Ghatte HF (2021). A hybrid of firefly and biogeography-based optimization algorithms for optimal design of steel frames. *Arabian Journal for Science and Engineering*, 46(5), 4703-4717.

Goldberg DE, Samtani MP (1986). Engineering optimization via genetic algorithm. *Proceedings of Ninth Conference on Electronic Computation. ASCE*, New York, NY, 471-482.

Govindaraj V, Ramasamy JV (2005). Optimum detailed design of reinforced concrete continuous beams using genetic algorithms. *Computers & structures*, 84(1-2), 34-48.

Holland JH (1975). Adaptation in Natural and Artificial Systems. University of Michigan Press, Ann Arbor, Michigan.

Karaboga D, Basturk B (2007). A powerful and efficient algorithm for numerical function optimization: artificial bee colony (ABC) algorithm. *Journal of Global Optimization*, 39(3), 459-471.

Kashani AR, Chiong R, Mirjalili S, Gandomi AH (2021). Particle swarm optimization variants for solving geotechnical problems: review and comparative analysis. *Archives of Computational Methods in Engineering*, 28(3), 1871-1927.

Kayabekir AE (2021). Effects of constant parameters on optimum design of axially symmetric cylindrical reinforced concrete walls. *The Structural Design of Tall and Special Buildings*, 30(6), e1838.

Kayabekir AE, Sayin B, Bekdaş G, Nigdeli SM (2017). Optimum carbon fiber reinforced polymer design for increasing shear capacity of RC beams. *3rd International Conference on Engineering and Natural Sciences* (*ICENS 2017*).

Kayabekir AE, Sayin B, Bekdaş G, Nigdeli SM (2018). The factor of optimum angle of carbon fiber reinforced polymers. *4th International Conference on Engineering and Natural Sciences* (*ICENS 2018*).

Kayabekir AE, Bekdaş G, Nigdeli SM (2019). Optimum design of T-beams using Jaya algorithm. *3rd International Conference on Engineering Technology and Innovation* (*ICETI*).

Kayabekir AE, Yücel M, Bekdaş G, Nigdeli SM (2020). Comparative study of optimum cost design of reinforced concrete retaining wall via metaheuristics. *Challenge Journal of Concrete Research Letters*, 11, 75-81.

Kennedy J, Eberhart RC (1995). Particle swarm optimization. *Proceedings of IEEE International Conference on Neural Networks No. IV*, November 27-December 1, Perth Australia, 1942–1948.

Kirkpatrick S, Gelatt CD, Vecchi MP (1983). Optimization by simulated annealing. *Science*, 220(4598), 671-680.

Martínez-Muñoz D, Martí JV, García J, Yepes V (2021). Embodied energy optimization of buttressed earth-retaining walls with hybrid simulated annealing. *Applied Sciences*, 11(4), 1800.

Mirjalili S, Mirjalili SM, Lewis A (2014). Grey wolf optimizer. *Advances in Engineering Software*, 69, 46-61.

Nigdeli SM, Bekdaş G (2016). Detailed optimum design of reinforced concrete frame structures. *WSEAS Transactions on Applied and Theoretical Mechanics*, 11, 220-228.

Nigdeli SM, Bekdas G, Kim S, Geem ZW (2015). A novel harmony search based optimization of reinforced concrete biaxial loaded columns. *Structural Engineering and Mechanics*, 54(6), 1097-1109.

Nigdeli SM, Bekdaş G, Yang XS (2018). Metaheuristic optimization of reinforced concrete footings. *KSCE Journal of Civil Engineering*, 22(11), 4555-4563.

Rafiq MY, Southcombe C (1998). Genetic algorithms in optimal design and detailing of reinforced concrete biaxial columns supported by a declarative approach for capacity checking. *Computers & Structures*, 69(4), 443-457.

Rao R (2016). Jaya: A simple and new optimization algorithm for solving constrained and unconstrained optimization problems. *International Journal of Industrial Engineering Computations*, 7(1), 19-34.

Rao RV, Savsani VJ, Vakharia DP (2011). Teaching–learning-based optimization: a novel method for constrained mechanical design optimization problems. *Computer-Aided Design*, 43(3), 303-315.

Shalchi Tousi M, Ghazavi M, Laali S (2021). Optimizing reinforced concrete cantilever retaining walls using Gases Brownian Motion Algorithm (GBMOA). *Journal of Soft Computing in Civil Engineering*, 5(1), 1-18.

Storn R, Price K (1997). Differential evolution–a simple and efficient heuristic for global optimization over continuous spaces. *Journal of Global Optimization*, 11(4), 341-359.

Timoshenko SP, Woinowsky-Krieger S (1984). Theory of Plates and Shells. 2nd Edition, McGraw-Hill, New York

Yang XS (2009). Firefly algorithms for multimodal optimization. *International Symposium on Stochastic Algorithms*, Springer, Berlin, Heidelberg, 169-178.

Yang XS (2010). A new metaheuristic bat-inspired algorithm. *Nature Inspired Cooperative Strategies for Optimization* (*NICSO 2010*), Springer, Berlin, Heidelberg, 65-74.

Yang XS (2012). Flower pollination algorithm for global optimization. *International conference on unconventional computing and natural computation*, Springer, Berlin, Heidelberg, 240-249.

Yang XS, Deb S (2010). Engineering optimisation by cuckoo search. *International Journal of Mathematical Modelling and Numerical Optimisation*, 1(4), 330-343.

Yepes V, Alcala J, Perea C, González-Vidosa F (2008). A parametric study of optimum earth-retaining walls by simulated annealing. *Engineering Structures*, 30(3), 821-830.

Yücel M, Kayabekir AE, Bekdaş G, Nigdeli SM, Kim S, Geem ZW (2021). Adaptive-Hybrid Harmony Search Algorithm for multi-constrained optimum eco-design of reinforced concrete retaining walls. *Sustainability*, 13(4), 1639.

Zhao J, Nguyen H, Nguyen-Thoi T, Asteris PG, Zhou J (2021). Improved Levenberg–Marquardt backpropagation neural network by particle swarm and whale optimization algorithms to predict the deflection of RC beams. *Engineering with Computers*, 1-23.

Challenge Journal of Structural Mechanics

Research Article

Experimental and numerical investigation of T section connections

Mahmut Kılıç [a,*], Abdulkadir Cüneyt Aydın [a], Merve Sağıroğlu [b], Mahyar Maali [b]

[a] *Department of Civil Engineering, Atatürk University, 25240 Erzurum, Turkey*

[b] *Department of Civil Engineering, Erzurum Technical University, 25050 Erzurum, Turkey*

ABSTRACT

The paper summarizes recent experimental research on determining the full-range behaviour of steel beam-to-column connections. Unlike the connection types in the literature, numerical modeling was done with various experiments to determine the behavior of two types of connection types. In these joints, T joints have been studied, but unlike the literature, T joint's element is made of plates; It was obtained from 1/2 IPE profile, not by welding. Thus, it is thought that the problems such as workmanship errors, break point formation and in situ welding failures, which occur in the welding of T joints, are eliminated. Necessary studies have been carried out to have sufficient information about the behavior of the T joint to be manufactured from the IPE profile and thus to provide the opportunity for its use. In the light of the data obtained, numerical modeling is done and the torque rotation relation and behavior of semi-rigid joints are numerically modeled. Thus, thanks to the calibrated model with the experiments, the closest results to the real behavior were obtained for the unexamined combinations.

ARTICLE INFO

Article history:
Received 4 October 2021
Revised 15 November 2021
Accepted 7 December 2021

Keywords:
T-type section
Beam-to-column connection
Experimental investigation
Numerical analysis
Semi-rigid design

1. Introduction

Beam-column joints play an important role in the behavior of frame systems. For more than half a century beam-column behavior has been studied both experimentally and theoretically. In calculation methods used in steel structures, beam column joints are considered to be hinged or rigid. According to these theories, there is no local rotation in the elements in rigid joints, and when a moment is influenced from outside, this moment is distributed in proportion to the rigidity of the elements. However, in reality, the joints are neither fully rigid nor fully articulated. In experimental studies conducted in recent years, it has been observed that more accurate results are obtained by accepting combinations as semi-rigid.

The bolted beam-to-column connections are an important part of steel frames. It is a significant issue to design beam-to-column connection of steel building's frames because the behavior of beam-to-column connection significantly influences the performance of the whole frame. Different connections types have been suggested and developed. Its bolted connections are usually applied to connect the beam to the column using some joint elements such as T-stubs, end-plates, and steel angles. Various parameters such as loading condition, connection details, and materials, affect the connection characteristics. The loading condition tests (Coelho and Bijlaard, 2007), and numerical analyses (Tagawa and Gurel, 2005; Kukreti and Zhou, 2006; Shi et al., 2008, Díaz et al., 2011) were carried out to evaluate the beam-to-column bolted connection. On the other hand, the stiffening of connections improve the performance of structures. The bolted connections of the beam-to-columns are usually designed by engineers as semi-rigid. (Tagawa and Liu, 2014; Tagawa et al., 2020).

The T-stub connections were experimentally investigated to the effect of beam-to-columns connection behavior. Its bolted connections often behave as semi-rigid connections so that their modeling requires many issues to be faced. Regarding the ability of beam-to-column joints in providing adequate plastic rotation supply and energy dissipation capacity for seismic design applications. A suitable joint semi-rigid design can lead to a plas-

* *Corresponding author*. Tel.: +90-442-231-4652 ; Fax: +90-442-231-4910 ; E-mail address: mahmut.kilic@atauni.edu.tr (M. Kılıç)
ISSN: 2149-8024 / DOI: https://doi.org/10.20528/cjsmec.2021.04.004

tic rotation supply compatible with the plastic rotation demand under seismic motion (Piluso and Rizzano, 2008). The information about the behavior of the joints achieved by experiments in order to understand the behavior of steel structures. However, different ways such as analytical, empirical, mechanical, numerical can be defined as the combination behavior (Batho and Rowan, 1934; Abdalla and Chen, 1995). The first application of bolts in steel structures had been started in 1950s, which was about the geometric and mechanical properties of rigid joints. From the 1950s to the present, different types have been investigated by researchers such as type of junction, upper and lower hull body type double-junction type, double-frame body joint type, single-frame body joint type, forehead plate joint type, beam-joint combination types. By comparing the results obtained from the models with the experimental data, it was stated that with the finite-element model, time and cost savings as well as the visual preparation of force and stress distributions to understand the behavior of the combination provided great advantages.

In recent years, many studies have been done on the analysis and design of space steel frames. In this research, they have developed a program for analyzing and designing space steel frames (Aydın et al., 2015a).

With stiffener and without stiffener, moment-rotation behavior was compared to the EN1993-1-8 specification (Aydın et al., 2015b).

The ductility of a joint (Ψ_j) is a property that reflects the length of the yield plateau of the moment-rotation response. The proposed definition of the ductility of a joint is the difference between the rotation value corresponding to the joint plastic resistance, $\theta_{M.Rd}$, and the total rotation capacity, θ_{Cd} (Aydın et al., 2015a, 2015b) (Fig. 2). Thus, the ductility of a joint relates the maximum rotation of the joint, θ_{Cd}, to the rotation value corresponding to the joint's plastic flexural resistance, $\theta_{M.Rd}$ (Maali et al., 2016, 2017, 2018a, 2018b).

2. Experimental Program

2.1. Test details

18 experiments were summarised in Table 1. In this study, T connections were obtained by 83 cuttings from standard IPE profiles, and a seat angle stiffener was selected. Fig. 1 shows the test details. Angle T connections were studied, but unlike the literature, not by welding, but by the 1/2 IPE profile. Thus, it is thought that problems such as workmanship errors that occur in the sources of T-connections, break-point formation, inadequate performance of on-site welding has been removed. T connections obtained from IPE profiles were experimented with using 1 and 2 rows of bolts. Thus, the effect of the row and number of bolts in the T profile body on the moment-rotation behavior was investigated.

In this research, each group compared with each other and other groups. The beam profile is from the IPE240 profile. The bolts are used in M8.8 quality and 14mm diameter, and finally the lower bracket L60*6 and 120mm width. Columns HEB160 is selected as standard.

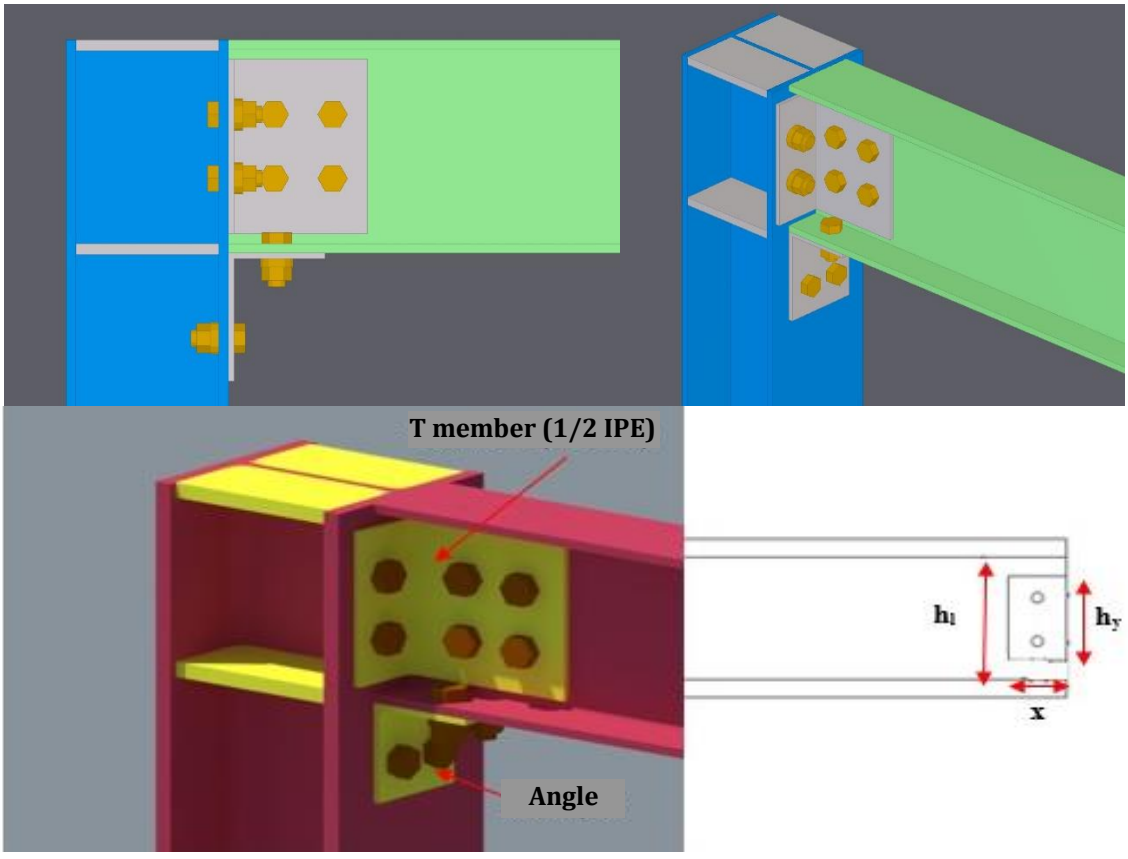

Fig. 1. Seat angle T connections.

Table 1. The geometry of the test.

Group	Specimen	$H_{max}=h_{y\,max}/h_1$	$H_{min}=h_{y\,min}/h_1$	$H_{mid}=h_{y\,med}/h_1$	X_{max} (mm)	X_{min} (mm)	½ T profile	Number of bolts
Angle T300	B240-T300-H_{max}-X_{max}-2-14-L60 (1)	1=22			215		IPE 300	2
	B240-T300-H_{min}-X_{max}-2-14-L60 (2)		0.63=14		215		IPE 300	2
	B240-T300-H_{mid}-X_{max}-2-14-L60 (3)			0.82=18	215		IPE 300	2
	B240-T300-H_{max}-X_{min}-1-14-L60 (4)	1=22				89	IPE 300	1
	B240-T300-H_{min}-X_{min}-1-14-L60 (5)		0.63=14			89	IPE 300	1
	B240-T300-H_{mid}-X_{min}-1-14-L60 (6)			0.82=18		89	IPE 300	1
Angle T270	B240-T270-H_{max}-X_{max}-2-14-L60 (7)	1=22			215		IPE 270	2
	B240-T270-H_{min}-X_{max}-2-14-L60 (8)		0.63=14		215		IPE270	2
	B240-T270-H_{mid}-X_{max}-2-14-L60 (9)			0.82=18	215		IPE 270	2
	B240-T270-H_{max}-X_{min}-1-14-L60 (10)	1=22				89	IPE 270	1
	B240-T270-H_{min}-X_{min}-1-14-L60 (11)		0.63=14			89	IPE270	1
	B240-T270-H_{mid}-X_{min}-1-14-L60 (12)			0.82=18		89	IPE270	1
Angle T240	B240-T240-H_{max}-X_{max}-2-14-L60 (13)	1=22			215		IPE240	2
	B240-T240-H_{min}-X_{max}-2-14-L60 (14)		0.63=14		215		IPE240	2
	B240-T240-H_{mid}-X_{max}-2-14-L60 (15)			0.82=18	215		IPE240	2
	B240-T240-H_{max}-X_{min}-1-14-L60 (16)	1=22				89	IPE240	1
	B240-T240-H_{min}-X_{min}-1-14-L60 (17)		0.63=14			89	IPE240	1
	B240-T240-H_{mid}-X_{min}-1-14-L60 (18)			0.82=18		89	IPE240	1

In the study, S235 steel grade, which is more common in the market, was preferred for all test samples. To observe the actual combined behaviour experimentally, the beam dimensions were chosen as 1500 mm. The specimens were subjected to a static force applied by a 900 kN hydraulic jack with a maximum piston stroke of 300 mm. Tests were performed under displacement control with a constant speed of 0.01 mm/s up to the collapse of the specimens. To prevent the lateral torsional buckling of the beam while loading, a two-column guidance device near the beam was provided. Fig. 2 shows that test setup.

The primary requirements of the instrumentation were the measurement of: The applied load (P); the displacements (DT) of the connection, beam, and angle T connection, the strains at the angle T connections. The results were collected using a data logging device that recorded all measurements and the load cells at one-second intervals. All the data were recorded for the duration of the test. Displacements were measured using linear variable displacement transducers with a maximum displacement of 300 mm. Two strain gauges (St) of TML YEFLA- 5 (maximum strain of 15-20%) used for calculated strain. The locations of LVDTs are given in Table 2.

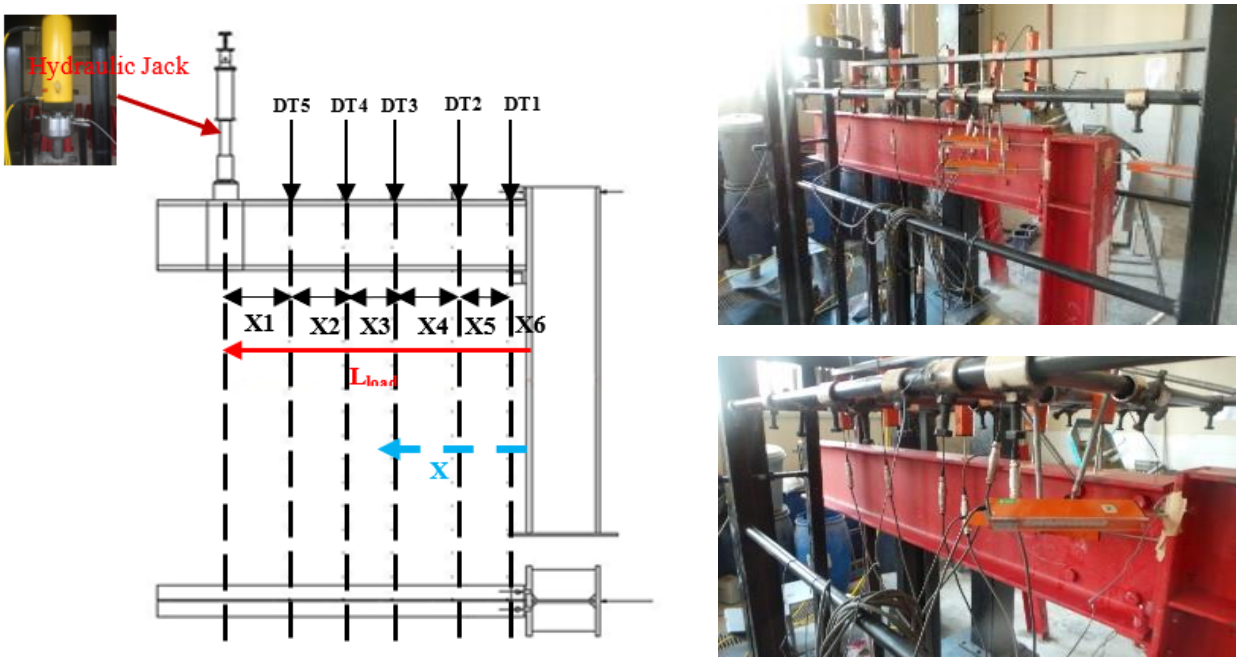

Fig. 2. Test setup.

Table 2. Locations of the displacement transducers (*DT* = LVDT).

Group	Specimen	X_1 (mm)	X_2 (mm)	X_3 (mm)	X_4 (mm)	X_5 (mm)	X_6 (mm)
Angle T300	B240-T300-H_{max}-X_{max}-2-14-L60 (1)	390	280	315	197	140	45
	B240-T300-H_{min}-X_{max}-2-14-L60 (2)	330	290	330	190	130	120
	B240-T300-H_{mid}-X_{max}-2-14-L60 (3)	330	295	320	200	130	90
	B240-T300-H_{max}-X_{min}-1-14-L60 (4)	280	320	270	200	145	115
	B240-T300-H_{min}-X_{min}-1-14-L60 (5)	255	328	293	190	160	130
	B240-T300-H_{mid}-X_{min}-1-14 -L60 (6)	305	332	285	195	155	88
Angle T270	B240-T270-H_{max}-X_{max}-2-14-L60 (7)	340	290	330	200	130	120
	B240-T270-H_{min}-X_{max}-2-14-L60 (8)	330	290	320	195	135	120
	B240-T270-H_{mid}-X_{max}-2-14-L60 (9)	335	295	320	190	135	100
	B240-T270-H_{max}-X_{min}-1-14-L60 (10)	320	330	175	110	335	110
	B240-T270-H_{min}-X_{min}-1-14-L60 (11)	290	335	300	205	130	14
	B240-T270-H_{mid}-X_{min}-1-14-L60 (12)	305	335	288	203	144	86
Angle T240	B240-T240-H_{max}-X_{max}-2-14-L60 (13)	390	290	320	193	13	45
	B240-T240-H_{min}-X_{max}-2-14-L60 (14)	320	285	325	195	135	130
	B240-T240-H_{mid}-X_{max}-2-14-L60 (15)	405	300	315	190	140	80
	B240-T240-H_{max}-X_{min}-1-14-L60 (16)	380	335	275	190	150	40
	B240-T240-H_{min}-X_{min}-1-14-L60 (17)	290	334	295	200	145	115
	B240-T240-H_{mid}-X_{min}-1-14-L60 (18)	298	325	294	203	140	100

2.2. Numerical models

The element types to be used in a combination to be analyzed in the ANSYS program should be defined beforehand. The staff in general; beam, plane, shell, solid and link (beam, plane, shell, solid and connection) elements are known for structural analysis. Models for this study are defined using solid elements. One of the most important steps in a finite-element analysis is the creation of the network structure. The ANSYS program has several mesh options available. In this study, the concentration of desired analyzes on the junction area, the regions where the stresses are intense and the junction area are kept smaller in the junction area and chosen larger in the girder and beam. The network structure can be seen in Fig. 3. Mesh sizing is important for accurate stress and displacement values. For this purpose, selected meshing type, the tetrahedron mesh divides various sizing meshes starting with 200 mm. When the stress and displacement values are stable, this mesh sizing can be applicable for FEM analysis.

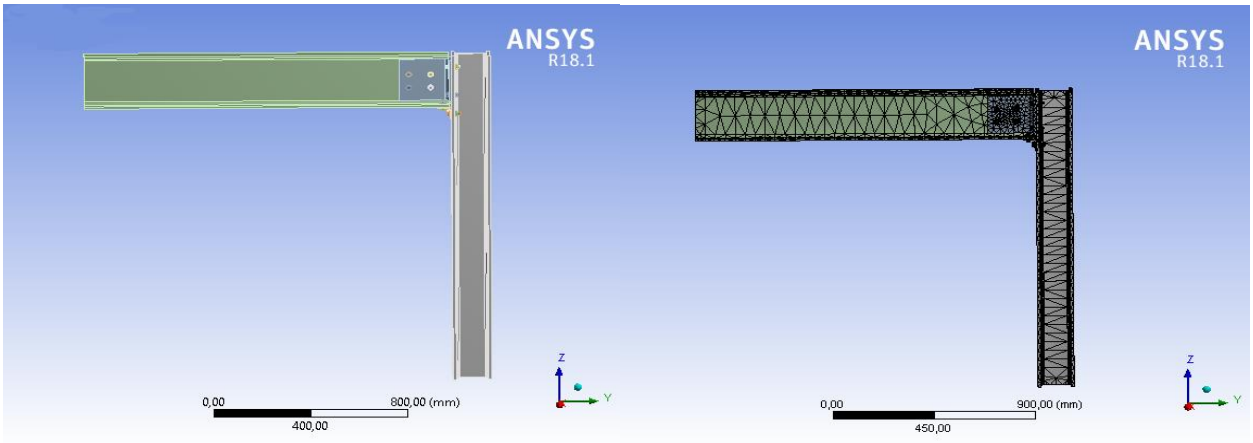

Fig. 3. Finite element modeling.

3. Experimental Results

In these experiments, experiments will be carried out by grouping as the width of the cornier (X), X_{max} containing 2 rows of bolts and X_{min} containing a single row of bolts. European and American Standards were taken into consideration while making this grouping selection. In these two groups, the H ratio, which we define as the ratio of corneal width h_y to beam trunk length h_1, is foreseen, and it is planned to make comparisons according to the H ratio in the experiment results. H values are divided into three groups as H_{max}, H_{mid} and H_{min}. Fig. 4 shows the major features of the moment rotation curve of Eurocode 3. The term "Knee-range" defined in Fig. 4 is the slope of the line drawn in the non-linear region of the moment-rotation curve.

3.1. T300, T270, T240 types double row bolted connection series

Fig. 5 shows the moment rotation curves of the T300, T270, and T240 angle groups. Fig. 6 shows that experiment models. Table 3 summarizes the experiment results.

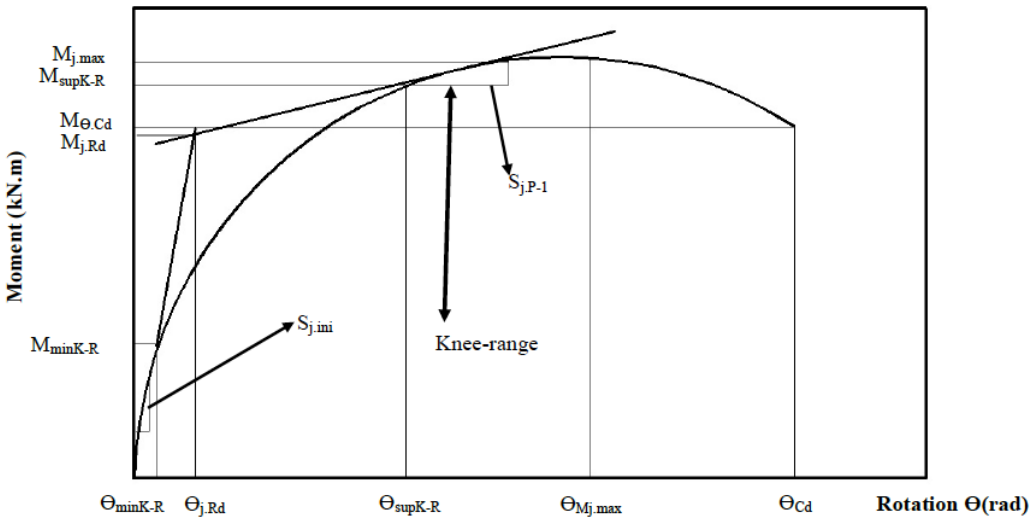

Fig. 4. Moment–rotation curve characteristics.

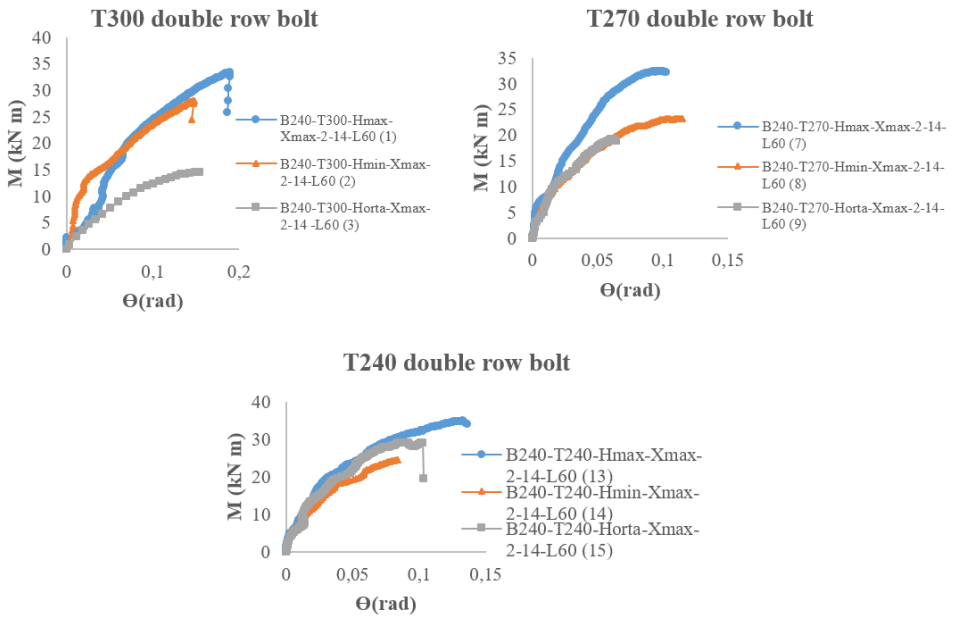

Fig. 5. T300-270-240 group moment-rotation curves of double row bolt tests.

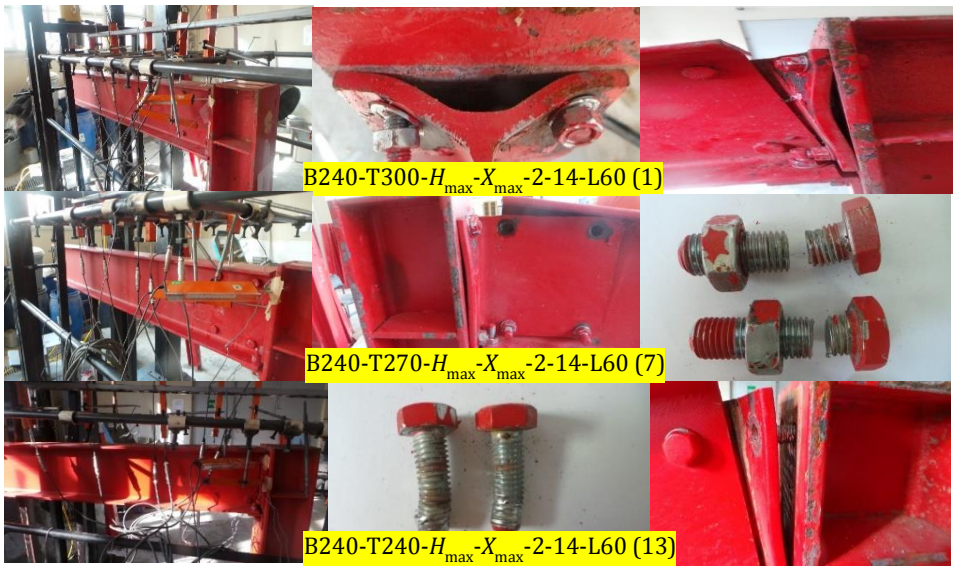

Fig. 6. Experiment models.

Table 3. Test results.

Experiment	Resistance (kN.m)			Stiffness (kN.m/rad)			Rotation (rad)					Ψ_j	$\Psi_{j.\max\ load}$	Energy dissipated (kN.m.rad)
	KR (knee-range)	$M_{j.Rd}$	$M_{j.\max}$	$M_{\theta Cd}$	$S_{j.\mathrm{ini}}$	$S_{j.p-1}$	$S_{j.\mathrm{ini}}/S_{j.p-1}$	$\theta_{M.Rd}$	$\theta_{\min.K.R}$	$\theta_{Msup.k.R}$	$\theta_{Mj.\max}$	θ_{Cd}			
B240-T300-$H_{\max}$-$X_{\max}$-2-14-L60 (1)	7.52-22.36	21.22	32.76	32.52	0.71	0.28	2.57	0.079	0.031	0.086	0.19	0.190	2.40	2.40	3.08
B240-T300-$H_{\min}$-$X_{\max}$-2-14-L60 (2)	10.13-19.16	13.88	27.95	27.48	2.33	0.29	7.88	0.018	0.014	0.067	0.15	0.150	8.33	8.33	2.06
B240-T300-H_{mid}-$X_{\max}$-2-14 -L60 (3)	3.5-12-86	11.95	14.47	14.47	1.22	0.17	7.19	0.069	0.018	0.110	0.15	0.150	2.17	2.17	1.08
B240-T270-$H_{\max}$-$X_{\max}$-2-14-L60 (7)	6.79-29.57	19.73	23.16	23.16	2.52	0.07	33.51	0.03	0.0091	0.093	0.11	0.110	5.00	5.00	1.64
B240-T270-$H_{\min}$-$X_{\max}$-2-14-L60 (8)	6.63-22.57	19.73	23.16	23.16	2.52	0.07	33.51	0.03	0.0091	0.093	0.11	0.110	3.66	3.66	1.27
B240-T270-H_{mid}-$X_{\max}$-2-14-L60 (9)	3.27-15.32	9.92	19.14	18.90	1.54	0.26	6.013	0.011	0.0031	0.040	0.062	0.064	5.82	5.82	0.60
B240-T240-$H_{\max}$-$X_{\max}$-2-14-L60 (13)	5.91-27.40	22.71	34.85	33.98	1.64	0.22	7.43	0.029	0.0057	0.065	0.13	0.140	4.83	4.48	2.38
B240-T240-$H_{\min}$-$X_{\max}$-2-14-L60 (14)	4.22-20.79	13.77	24.5	24.42	1.90	0.21	8.91	0.012	0.0034	0.058	0.08	0.083	6.92	6.66	1.01
B240-T240-H_{mid}-$X_{\max}$-2-14-L60 (15)	7.37-27.03	23.01	28.93	28.93	1.80	0.15	12.26	0.024	0.0064	0.068	0.102	0.102	4.25	4.25	1.47

The plastic flexural resistance, $M_{j.Rd}$,which corresponds to the intersection point of the revious two regression lines obtained for the initial stiffness ($S_{j.\mathrm{ini}}$) and for the post-limit stiffness ($S_{j.p-1}$) and its corresponding rotation $\theta_{M.Rd}$;

The maximum bending moment, $M_{j.\max}$, and its corresponding rotation, $\theta_{M.j.\max}$;

The knee-range of the $M-\theta$ curve, which is defined as the transition zone between the initial and post-limit stiffness, with its lower boundary at $M_{\min.k-R}$ and rotation $\theta_{\min.k-R}$, and with its upper limit at $M_{\sup.k-R}$ and rotation $\theta_{\sup.k-R}$;

The bending moment capacity, $M_{\theta.Cd}$, and its corresponding rotation capacity, θ_{cd}.

The ductility of a joint (Ψ_j) is a property that reflects the length of the yield plateau of the moment-rotation response. The proposed definition of the ductility of a joint is the difference between the rotation value corresponding to the joint plastic resistance, $\theta_{M.Rd}$, and the total rotation capacity, θ_{Cd}, Thus, the ductility of a joint relates the maximum rotation of the joint, θ_{Cd}, to the rotation value corresponding to the joint's plastic flexural resistance, $\theta_{M.Rd}$.

Comparisons of T300, T270 and T240 type connection combinations in their own groups are summarized in Table 4.

Moment-strain graphics of the experiments are shown in Figure 7.

Table 5 shows the comparison of T300, T270, T240 Double row bolted connections according to $H_{\max}$, $H_{\min}$, H_{mid} state.

Table 4. Comparison of T300, T270, T240 double row bolted joints in their own groups.

Exp.	Resistance (kN.m)			Stiffness (kN.m/rad)			Rotation (rad)					Ψ_j	$\Psi_{j.\max\ load}$	Energy dissipated (kN.m.rad)
	$M_{j.Rd}$	$M_{j.\max}$	$M_{\theta Cd}$	$S_{j.\mathrm{ini}}$	$S_{j.p-1}$	$S_{j.\mathrm{ini}}/S_{j.p-1}$	$\theta_{M.Rd}$	$\theta_{\min.K.R}$	$\theta_{Msup.k.R}$	$\theta_{Mj.\max}$	θ_{Cd}			
1--2	34.590	14.683	15.498	-228.169	-3.571	-206.615	77.215	54.839	22.093	21.053	21.053	-247.083	-247.083	33.117
1--3	43.685	55.830	55.504	-71.831	39.286	-179.767	12.658	41.935	-27.907	21.053	21.053	9.583	9.583	64.935
2--3	13.905	48.229	47.344	47.639	41.379	8.756	-283.333	-28.571	-64.179	0.000	0.000	73.950	73.950	47.573
7--8	0.000	0.000	0.000	0.000	0.000	0.000	0.000	0.000	0.000	0.000	0.000	26.800	26.800	22.561
7--9	49.721	17.358	18.394	38.889	-271.429	82.056	63.333	65.934	56.989	43.636	41.818	-16.400	-16.400	63.415
8--9	49.721	17.358	18.394	38.889	-271.429	82.056	63.333	65.934	56.989	43.636	41.818	-59.016	-59.016	52.756
13--14	39.366	29.699	28.134	-15.854	4.545	-19.919	58.621	40.351	10.769	38.462	40.714	-43.271	-48.661	57.563
13--15	-1.321	16.987	14.862	-9.756	31.818	-65.007	17.241	-12.281	-4.615	21.538	27.143	12.008	5.134	38.235
14--15	-67.102	-18.082	-18.468	5.263	28.571	-37.598	-100.000	-88.235	-17.241	-27.500	-22.892	38.584	36.186	-45.545

Table 5. Comparison of T300, T270, T240 double row bolted connections according to $H_{\max}$, $H_{\min}$, H_{mid} state.

Exp.	Resistance (kN.m)			Stiffness (kN.m/rad)			Rotation (rad)					Ψ_j	$\Psi_{j.\max\ load}$	Energy dissipated (kN.m.rad)
	$M_{j.Rd}$	$M_{j.\max}$	$M_{\theta Cd}$	$S_{j.\mathrm{ini}}$	$S_{j.p-1}$	$S_{j.\mathrm{ini}}/S_{j.p-1}$	$\theta_{M.Rd}$	$\theta_{\min.K.R}$	$\theta_{Msup.k.R}$	$\theta_{Mj.\max}$	θ_{Cd}			
1--7	7.022	29.304	28.782	-254.930	75.000	-1203.891	62.025	70.645	-8.140	42.105	42.105	-108.333	-108.333	46.753
1--13	-7.022	-6.380	-4.490	-130.986	21.429	-189.105	63.291	81.613	24.419	31.579	26.316	-101.250	-86.667	22.727
7--13	-15.104	-50.475	-46.718	34.921	-214.286	77.828	3.333	37.363	30.108	-18.182	-27.273	3.400	10.400	-45.122
2--8	-42.147	17.138	15.721	-8.155	75.862	-325.254	-66.667	35.000	-38.806	26.667	26.667	56.062	56.062	38.350
2--14	0.793	12.343	11.135	18.455	27.586	-13.071	33.333	75.714	13.433	46.667	44.667	16.927	20.048	50.971
8--14	30.208	-5.786	-5.440	24.603	-200.000	73.411	60.000	62.637	37.634	27.273	24.545	-89.071	-81.967	20.472
3--9	16.987	-32.274	-30.615	-26.230	-52.941	16.370	84.058	82.778	63.636	58.667	57.333	-168.203	-168.203	44.444
3--15	-92.552	-99.931	-99.931	-47.541	11.765	-70.515	65.217	64.444	38.182	32.000	32.000	-95.853	-95.853	-36.111
9--15	-131.956	-51.149	-53.069	-16.883	42.308	-103.892	-118.182	-106.452	-70.000	-64.516	-59.375	26.976	26.976	-145.000

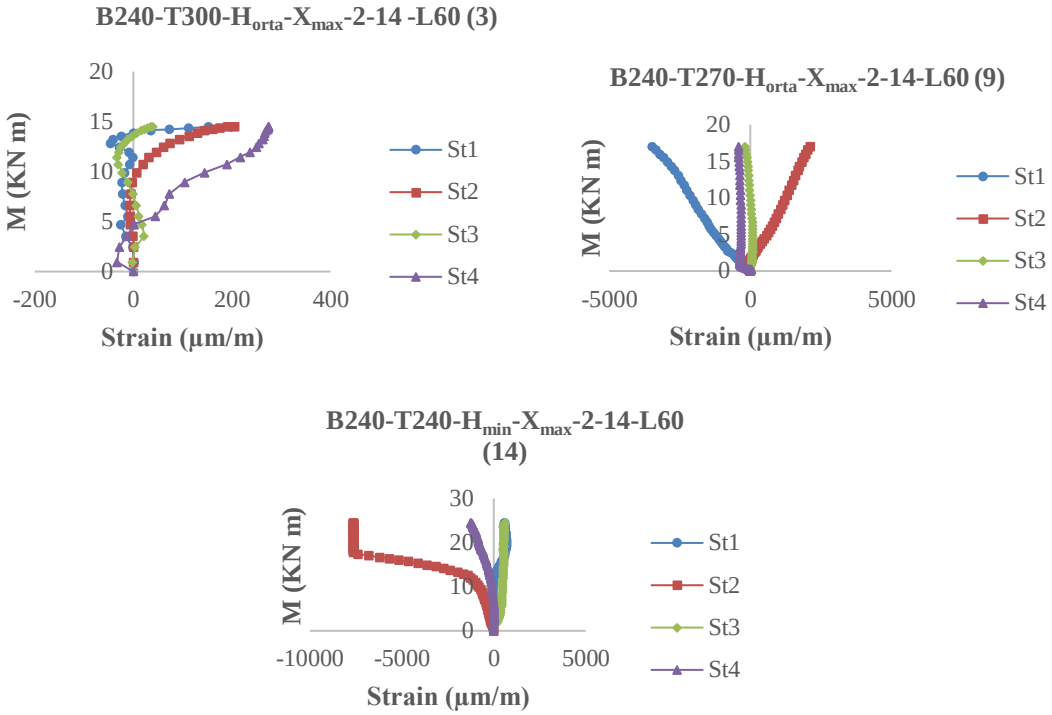

Fig. 7. Moment–strain curves for T300-T270 and T240 type double row bolts.

3.1.1. Failure mechanism

According to Eurocode 3, three types of breaking performance have been proposed for face plate joints. The first kind of breakage is that there is only deformation in the plate (Fig. 8a). The second kind of breakage is deformation and bolt breakage (Fig. 8b), and the third type is just bolt breakage (Fig. 8c). As seen in Fig. 8, this kind of cutting and breaking is the first kind of breaking situation. In other words, in the proposed combination, the first kind of breakage occurs.

It is observed that $M_{j.Rd}$, $M_{j.max}$ and $M_{\theta cd}$ value increased in all groups with the increase of H value. Looking at the $M_{j.Rd}$, $M_{j.max}$ and $M_{\theta cd}$ values; it is seen that the highest value in the T300 and T270 group is in the H_{max}-X_{max} group and the T240 group it is also in H_{max}-X_{max} and H_{mid}-X_{max}. Looking at the T300 and T270 groups, it is seen that H_{mid} values are smaller than H_{min} values. That is, as the thickness (t) of the joint increases, H_{max} joint types should be selected. Considering the combinations of H_{min} and H_{mid}, H_{min} should be chosen since it is economically more convenient. As the H value increases, $M_{j.Rd}$, $M_{j.max}$ and $M_{\theta cd}$ value increase.

Fig. 8. Collapse models.

The highest $M_{j.Rd}$ change was seen as an increase of 49.72% when the H_{max}-X_{max} and H_{mid}-X_{max} groups were compared in the T270 group.

The highest $M_{j.max}$ change was observed in the H_{max}-X_{max} group in the T300 group and a 55.50% increase in the H_{mid}-X_{max} group.

The highest $M_{\theta cd}$ change was observed in the H_{max}-X_{max} group in the T300 group and a 55.50% increase in the H_{mid}-X_{max} group.

As the thickness of the T joint element increases, the stiffness decreases. H_{mid} values were found to be the largest. So they are the most rigid connections.

$\theta_{M.Rd}$ value increases as T combination thickness and H increase. The highest variation was seen in the H_{max}-X_{max} and H_{min}-X_{max} groups of the T300 group, with an increase of 77.21%.

$\Theta_{Mj.max}$ value increases as the T connection's thickness increases. The highest change was in the H_{max}-X_{max} and H_{mid}-X_{max} group in the T270 group, at +43.63%.

The θ_{Cd} value varies depending on the H value. This change is directly proportional. As the T connection's thickness increases, θ_{Cd} value increases. The highest change was in the H_{max}-X_{max} and H_{mid}-X_{max} group in the T270 group, at +41.81%.

The BB value decreased as the thickness increased. H_{min} values were found to be higher than H_{max} and H_{mid} values. If we want the Ψ_j values to be high, it is recommended to use H_{min}.

It is seen that $\Psi_{j.max\ load}$ value decreases with increasing thickness. It was observed that H_{min} value was higher than H_{max} and H_{mid} value. If we want the CC values to be too high, it is recommended to use H_{min} profile.

As the thickness increased, an increase in energy dissipated values was observed. When each group is evaluated within itself, energy dissipated increased as H increased. The best results are achieved when the wall thickness is high, and the H value is maximum.

3.1.2. Finite element models

The model pictures of finite elements for experiments using T300, T270 and T240 double row bolts are shown in Fig. 9. The results obtained from the curves are given in Table 6. Comparison of finite elements with experimental results is given in Table 7.

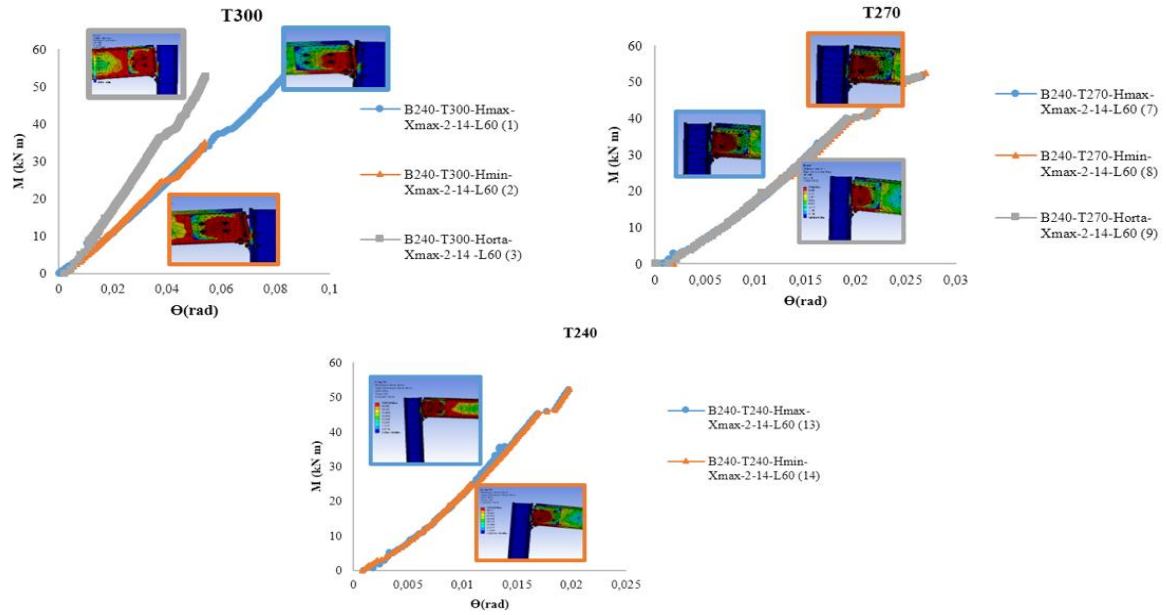

Fig. 9. T300-270-240 group moment-rotation curves of double row bolt finite element models.

Table 6. Model results of T300, T270, T240 double row bolt finite element models.

Experiment	Resistance (kN.m)			Stiffness (kN.m/rad)				Rotation (rad)					Ψ_j	$\Psi_{j.max\ load}$	Energy dissipated (kN.m.rad)
	KR (knee-range)	$M_{j.Rd}$	$M_{j.max}$	$M_{\theta Cd}$	$S_{j.ini}$	$S_{j.p-1}$	$S_{j.ini}/S_{j.p-1}$	$\theta_{M.Rd}$	$\theta_{min.KR}$	$\theta_{Msup.kR}$	$\theta_{Mj.max}$	θ_{Cd}			
B240-T300-H_{max}-X_{max}-2-14-L60 (1)	36.72-38.75	37.85	52.45	52.45	1.07	1.40	0.764	0.041	0.039	0.043	0.083	0.083	2.024	2.024	2.1767
B240-T300-H_{min}-X_{max}-2-14-L60 (2)	24.80-25.40	24.95	35.01	35.01	0.88	0.66	1.333	0.039	0.039	0.041	0.053	0.053	1.359	1.359	0.9278
B240-T300-H_{mid}-X_{max}-2-14 -L60 (3)	37.20-38.29	37.50	54.69	52.69	0.77	0.70	1.100	0.061	0.058	0.063	0.054	0.054	0.885	0.885	1.4226
B240-T270-H_{max}-X_{max}-2-14-L60 (7)	39.05-47.64	40.51	51.85	51.85	0.92	0.49	1.878	0.021	0.019	0.023	0.026	0.026	1.238	1.238	0.6741
B240-T270-H_{min}-X_{max}-2-14-L60 (8)	22.50-29.75	23.63	52.50	52.50	0.92	0.77	1.195	0.014	0.013	0.015	0.026	0.026	1.857	1.857	0.6825
B240-T270-H_{mid}-X_{max}-2-14-L60 (9)	39.15-47.54	40.50	51.40	51.40	0.92	0.49	1.878	0.021	0.018	0.021	0.025	0.025	1.190	1.190	0.6425
B240-T240-H_{max}-X_{max}-2-14-L60 (13)	34.24-35.76	34.70	52.09	52.09	0.99	0.74	1.338	0.014	0.0139	0.0143	0.019	0.019	1.357	1.357	0.4949
B240-T240-H_{min}-X_{max}-2-14-L60 (14)	45.33-46.84	46.33	52.38	52.38	0.79	0.73	1.082	0.0179	0.017	0.018	0.019	0.019	1.061	1.061	0.4976

Table 7. T300, T270, T240 type double-row finite element model and comparison of experimental results.

Exp.	Resistance (kN.m)			Stiffness (kN.m/rad)			Rotation (rad)					Ψ_j	$\Psi_{j.\max\ load}$	Energy dissipated (kN.m.rad)
	$M_{j.Rd}$	$M_{j.\max}$	$M_{\Theta Cd}$	$S_{j.\mathrm{ini}}$	$S_{j.p-1}$	$S_{j.\mathrm{ini}}/S_{j.p-1}$	$\Theta_{M.Rd}$	$\Theta_{\min.K.R}$	$\Theta_{Msup.k.R}$	$\Theta_{Mj.\max}$	Θ_{Cd}			
1--1	1.78	1.60	1.61	1.51	5.00	0.30	0.52	1.26	0.50	0.44	0.44	0.84	0.84	0.71
2--2	1.80	1.25	1.27	0.38	2.28	0.17	2.17	2.79	0.61	0.35	0.35	0.16	0.16	0.45
3--3	3.14	3.78	3.64	0.63	4.12	0.15	0.88	3.22	0.57	0.36	0.36	0.41	0.41	1.32
7--7	2.05	2.24	2.24	0.37	7.00	0.06	0.70	2.09	0.25	0.24	0.24	0.25	0.25	0.41
8--8	1.20	2.27	2.27	0.37	11.00	0.04	0.47	1.43	0.16	0.24	0.24	0.51	0.51	0.54
9--9	4.08	2.69	2.72	0.60	1.88	0.31	1.91	5.81	0.53	0.40	0.39	0.20	0.20	1.07
13--13	1.53	1.49	1.53	0.60	3.36	0.18	0.48	2.44	0.22	0.15	0.14	0.28	0.30	0.21
14--14	3.36	2.14	2.14	0.42	3.48	0.12	1.49	5.00	0.31	0.24	0.23	0.15	0.16	0.49

T300 types double row bolt connections (B240-T300-$H_{\max}$-$X_{\max}$-2-14-L60 (1), B240-T300-$H_{\min}$-$X_{\max}$-2-14-L60 (2) and B240-T300-H_{mid}-$X_{\max}$-2-14-L60 (3)) average experiment and numerical analysis results were compared. As a result of the comparison, a multiplier was created between the experiment results and the numerical results. These values are determined as 2.24 for $M_{j.Rd}$, 2.21 for $M_{j.\max}$, 2.18 for $M_{\Theta Cd}$, 0.21 for $S_{j.\mathrm{ini}}/S_{j.p-1}$, 1.19 for $\Theta_{M.Rd}$ and 0.38 for $\Theta_{Mj.\max}$ and Θ_{Cd}. For Ψ_j and $\Psi j._{\max\ load}$ value is rate 0.47. For Energy Dissipated is rate 0.82.

T270 types double row bolt connections (B240-T270-$H_{\max}$-$X_{\max}$-2-14-L60 (7), B240-T270-$H_{\min}$-$X_{\max}$-2-14-L60 (8) and B240-T270-H_{mid}-$X_{\max}$-2 -14-L60 (9)) average experiment and numerical analysis results were compared. For $M_{j.Rd}$ value, numerical analysis results are obtained by multiplying the experiment results by 2.44. For $M_{j.\max}$ value rate is 2.41. For $S_{j.\mathrm{ini}}/S_{j.p-1}$, this value was calculated as 0.13. The numerical analysis value of $\Theta_{M.Rd}$ is obtained by multiplying the experiment result by 1.03. The experiment $\Theta_{Mj.\max}$ and Θ_{Cd} value is multiplied by 0.29 to obtain the numerical analysis. Numerical analysis results can be found by multiplying the experimental Ψ_j and $\Psi j._{\max\ load}$ values by 0.32. For Energy Dissipated is rate 0.67.

T240 type single row bolted connections (B240-T240-$H_{\max}$-$X_{\max}$-2-14-L60 (13) and B240-T240-$H_{\min}$-$X_{\max}$-2-14-L60 (14)) average experiment and numerical analysis results were compared. When the experiment A value is multiplied by 2.45, the result of numerical analysis is obtained. It happened when $M_{j.\max}$ was multiplied by 1.82. At $M_{\Theta Cd}$, numerical analysis results were 1.84 times the experiment results. In $S_{j.\mathrm{ini}}/S_{j.p-1}$, this value was calculated as 0.15. Considering the $\Theta_{Mj.\max}$ and Θ_{Cd} values, the ratio between experiment and numerical results is 0.19. When we look at the experimental Ψ_j and numerical Ψ_j ratios, this value was found to be 0.22. When the experiment $\Psi j._{\max\ load}$ value is multiplied by 0.22, the result of numerical analysis is obtained. Energy Dissipated; experiment results are multiplied by 0.35 and numerical analysis results are obtained.

3.2. T300, T270, T240 types single row bolted connection series.

Fig. 10 shows the moment-rotation curves of the T300, T270, and T240 angle groups. Fig. 11 shows the experiment models. Table 8 summarizes the experiment results. Comparison of experiment results of angle group combinations is shown in Table 9.

Moment-strain graphics of the experiments are shown in Fig. 12.

The values obtained from the strain gauges placed at the 1, 2, 3 and 4 points of the samples are shown in Fig. 12. Since the value could not be obtained at 4 points of the B240-T300-$H_{\min}$-$X_{\min}$-1-14-L60 sample, it is not presented in the graph.

Table 10 shows that comparison of T300, T270, T240 single row bolted connections according to $H_{\max}$, $H_{\min}$, H_{mid} states.

Table 8. Test results of T300, T270, T240 single row bolt combinations.

Experiment	Resistance (kN.m)			Stiffness (kN.m/rad)				Rotation (rad)					Ψ_j	$\Psi_{j.\max\ load}$	Energy dissipated (kN.m.rad)
	KR (knee-range)	$M_{j.Rd}$	$M_{j.\max}$	$M_{\Theta Cd}$	$S_{j.\mathrm{ini}}$	$S_{j.p-1}$	$S_{j.\mathrm{ini}}/S_{j.p-1}$	$\Theta_{M.Rd}$	$\Theta_{\min.K.R}$	$\Theta_{Msup.k.R}$	$\Theta_{Mj.\max}$	Θ_{Cd}			
B240-T300-$H_{\max}$-$X_{\min}$-1-14 —L60 (4)	2.36-10.53	10.17	13.57	13.45	0.53	0.35	1.49	0.057	0.016	0.059	0.081	0.081	1.42	1.42	0.54
B240-T300-$H_{\min}$-$X_{\min}$-1-14-L60 (5)	3.47-15.08	8.80	16.63	16.63	3.18	0.26	12.33	0.0064	0.0028	0.054	0.066	0.066	10.31	10.31	0.55
B240-T300-H_{mid}-$X_{\min}$-1-14 —L60 (6)	0.94-11.25	8.37	16.82	16.82	0.58	0.44	1.31	0.042	0.005	0.057	0.092	0.092	2.19	2.19	0.77
B240-T270-$H_{\max}$-$X_{\min}$-1-14-L60 (10)	5.48-6.71	5.48	15.67	15.67	6.1	0.37	16.48	0.021	0.0021	0.015	0.095	0.095	4.23	4.23	0.74
B240-T270-$H_{\min}$-$X_{\min}$-1-14-L60 (11)	2.64-8.98	2.99	14.58	14.58	0.89	0.49	1.78	0.014	0.011	0.056	0.101	0.101	7.21	7.21	1.47
B240-T270-H_{mid}-$X_{\min}$-1-14-L60 (12)	2.76-8.32	3.82	15.67	14.91	0.25	0.71	0.35	0.034	0.028	0.051	0.078	0.079	2.32	2.29	0.59
B240-T240-$H_{\max}$-$X_{\min}$-1-14-L60 (16)	2.60-13.67	8.39	16.86	16.66	0.75	0.44	1.70	0.058	0.02	0.11	0.156	0.156	2.68	2.58	1.29
B240-T240-$H_{\min}$-$X_{\min}$-1-14-L60 (17)	4.66-12.95	11.72	13.39	13.31	1.40	0.071	19.44	0.019	0.0077	0.056	0.063	0.063	3.36	3.36	0.42
B240-T240-H_{mid}-$X_{\min}$-1-14-L60 (18)	9.00-16.051	9.00	16.80	16.41	1.68	0.41	4.11	0.027	0.027	0.068	0.078	0.079	2.92	2.88	0.65

Table 9. T300, T270, T240 Comparison of test results of single row bolted joints (own groups).

Exp.	Resistance (kN.m)			Stiffness (kN.m/rad)			Rotation (rad)					Ψ_j	$\Psi_{j.\max load}$	Energy dissipated (kN.m.rad)
	$M_{j.Rd}$	$M_{j.\max}$	$M_{\theta Cd}$	$S_{j.ini}$	$S_{j.p-1}$	$S_{j.ini}/S_{j.p-1}$	$\theta_{M.Rd}$	$\theta_{\min.K.R}$	$\theta_{Msup.k.R}$	$\theta_{Mj.\max}$	θ_{Cd}			
4—5	13.471	-22.550	-23.643	-500.000	25.714	-727.517	88.772	82.500	8.475	18.519	18.519	-626.056	-626.056	-1.852
4—6	17.699	-23.950	-25.056	-9.434	-25.714	12.081	26.316	68.750	3.390	-13.580	-13.580	-54.225	-54.225	-42.593
5—6	4.886	-1.143	-1.143	81.761	-69.231	89.376	-556.250	-78.571	-5.556	-39.394	-39.394	78.758	78.758	-40.000
10—11	45.438	6.956	6.956	85.410	-32.432	89.199	-566.667	-423.810	-273.333	-6.316	-6.316	84.059	84.059	-98.649
10—12	30.292	0.000	4.850	95.902	-91.892	97.876	-1519.048	-1233.333	-240.000	17.895	16.842	94.871	94.937	20.270
11—12	-27.759	-7.476	-2.263	71.910	-44.898	80.337	-142.857	-154.545	8.929	22.772	21.782	67.822	68.239	59.864
16—17	-39.690	20.581	20.108	-86.667	83.864	-1043.529	67.241	61.500	49.091	59.615	59.615	-25.373	-30.233	67.442
16—18	-7.271	0.356	1.501	-124.000	6.818	-141.765	53.448	-35.000	38.182	50.000	49.359	-8.955	-11.628	49.612
17—18	23.208	-25.467	-23.291	-20.000	-477.465	78.858	-42.105	-250.649	-21.429	-23.810	-25.397	13.095	14.286	-54.762

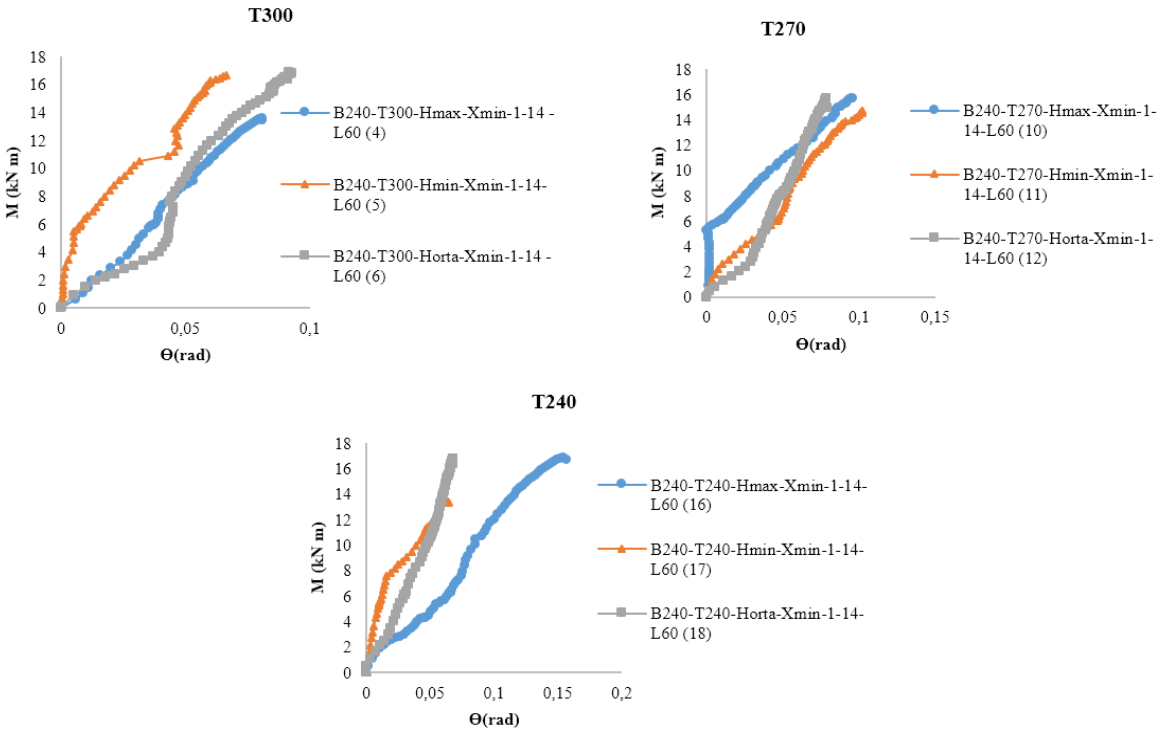

Fig. 10. T300-270-240 group moment-rotation curves of single row bolt tests.

Fig. 11. Experimental models.

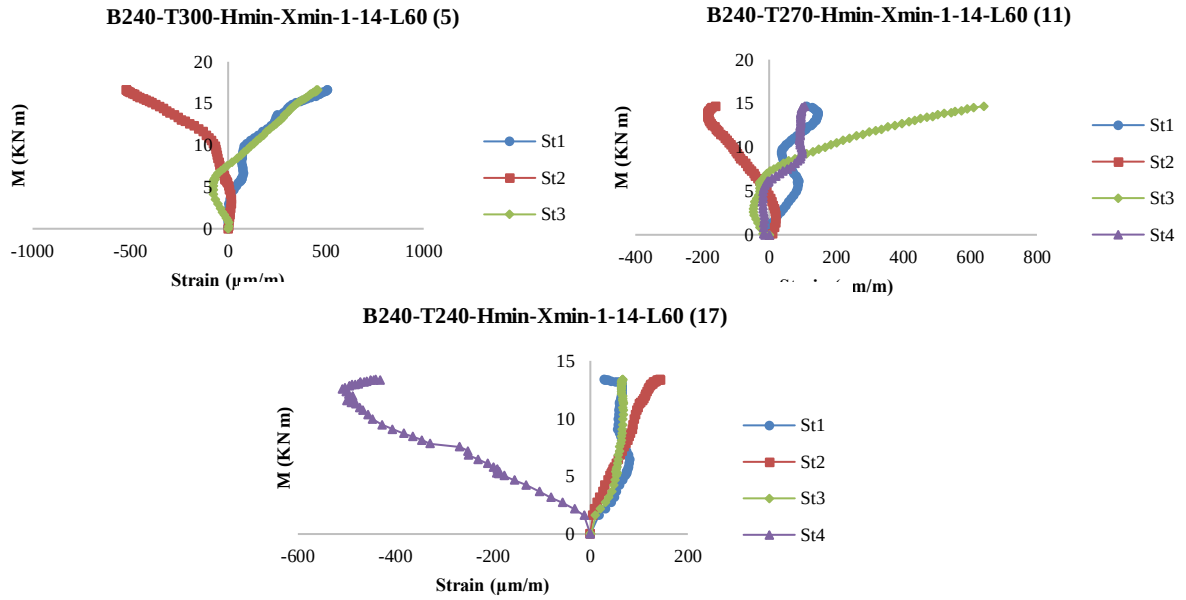

Fig. 12. Moment–strain curves for T300-T270 and T240 type single row bolts.

Table 10. T300, T270, T240 comparison of single row bolted joints according to H_{max}, H_{min}, H_{mid} states.

Exp.	Resistance (kN.m)			Stiffness (kN.m/rad)			Rotation (rad)					Ψ_j	$\Psi_{j,max\ load}$	Energy dissipated (kN.m.rad)
	$M_{j,Rd}$	$M_{j,max}$	$M_{\theta Cd}$	$S_{j,ini}$	$S_{j,p-1}$	$S_{j,ini}/S_{j,p-1}$	$\theta_{M,Rd}$	$\theta_{min,KR}$	$\theta_{Msup,kR}$	$\theta_{Mj,max}$	θ_{Cd}			
4--10	46.116	-15.475	-16.506	-1050.943	-5.714	-1006.040	96.316	86.875	74.576	-17.284	-17.284	-3085.21	-3085.211	-37.037
4--16	17.502	-24.245	-23.866	-41.509	-25.714	-14.094	-1.754	-25.000	-86.441	-92.593	-92.593	-88.732	-81.690	-138.889
10--16	-53.102	-7.594	-6.318	87.705	-18.919	89.684	-2661.905	-852.381	-633.333	-64.211	-64.211	94.075	94.296	-74.324
5--11	66.023	12.327	12.327	72.013	-88.462	85.564	-118.750	-292.857	-3.704	-53.030	-53.030	30.068	30.068	-167.273
5--17	-33.182	19.483	19.964	55.975	72.692	-57.664	-196.875	-175.000	-3.704	4.545	4.545	67.410	67.410	23.636
11--17	-291.973	8.162	8.711	-57.303	85.510	-992.135	-35.714	30.000	0.000	37.624	37.624	53.398	53.398	71.429
6--12	54.361	6.837	11.356	56.897	-61.364	73.282	19.048	-460.000	10.526	15.217	14.130	-5.936	-4.566	23.377
6--18	-7.527	0.119	2.438	-189.655	6.818	-213.740	35.714	-440.000	-19.298	15.217	14.130	-33.333	-31.507	15.584
12--18	-135.602	-7.211	-10.060	-572.000	42.254	-1074.286	20.588	3.571	-33.333	0.000	0.000	-25.862	-25.764	-10.169

3.2.1. Failure mechanism

According to Eurocode 3, three types of breaking performance have been proposed for face plate joints. The first kind of breakage is that there is only deformation in the plate (Fig. 13a). The second kind of breakage is deformation and bolt breakage (show that Fig. 13b), and the third type is just bolt breakage (Fig. 13c). As seen in Fig. 13, this kind of cutting and breaking is the first kind of breaking situation. In other words, in the proposed combination, the first kind of breakage occurs.

Fig. 13. Collapse models.

Looking at $M_{j.Rd}$ values; T300 largest value in the group appears to be in H_{max}-X_{min} group. Referring to these values in the group appears to be in the H_{min}-X_{min} group T270. With the increase of H value, BB value increased in all groups. The highest change was seen in the T270 group when the H_{max}-X_{min} and H_{min}-X_{min} groups were compared, an increase of 45.43%.

3.2.2. Finite element models

Fig. 14 shows the moment-rotation curves obtained by the finite element's model. The results obtained from the curves are given in Table 11. Comparison of finite elements with experiment results is given in Table 12.

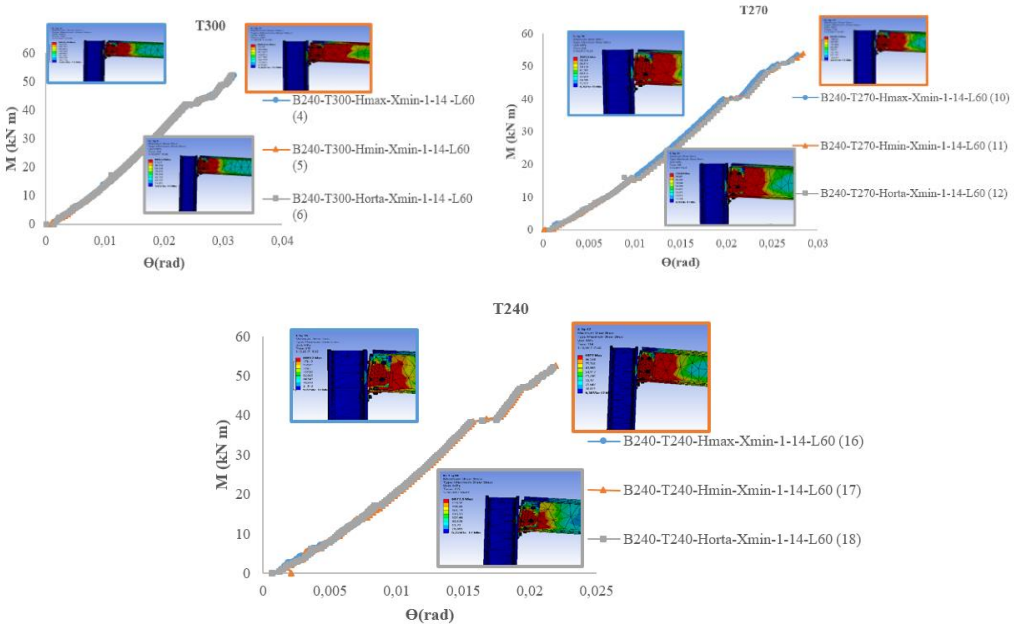

Fig. 14. T300, T270 and T240 group moment-rotation curves of single row bolt finite element models.

Table 11. T300, T270, T240 type single row bolt finite element model experiment results.

Experiment	Resistance (kN.m)			Stiffness (kN.m/rad)				Rotation (rad)					Ψ_j	$\Psi_{j.max\ load}$	Energy dissipated (kN.m.rad)
	KR (knee-range)	$M_{j.Rd}$	$M_{j.max}$	$M_{\theta Cd}$	$S_{j.ini}$	$S_{j.p-1}$	$S_{j.ini}/S_{j.p-1}$	$\theta_{M.Rd}$	$\theta_{min.K.R}$	$\theta_{Msup.k.R}$	$\theta_{Mj.max}$	θ_{Cd}			
B240-T300-H_{max}-X_{min}-1-14 -L60 (4)	41.75-48.64	42.79	52.08	52.08	1.05	0.61	1.721	0.025	0.023	0.029	0.032	0.032	1.280	1.280	0.8333
B240-T300-H_{min}-X_{min}-1-14-L60 (5)	41.75-48.64	42.79	51.03	51.03	1.05	0.61	1.721	0.025	0.023	0.029	0.031	0.031	1.240	1.240	0.7910
B240-T300-H_{mid}-X_{min}-1-14 -L60 (6)	41.75-48.69	42.79	52.09	52.09	1.05	0.61	1.721	0.025	0.023	0.029	0.031	0.031	1.240	1.240	0.8074
B240-T270-H_{max}-X_{min}-1-14-L60 (10)	39.15-40.05	43.65	53.57	53.57	0.93	0.51	1.824	0.021	0.02	0.021	0.027	0.027	1.286	1.286	0.7232
B240-T270-H_{min}-X_{min}-1-14-L60 (11)	39.15-42.75	40.95	54.00	54.00	0.85	0.70	1.214	0.021	0.02	0.022	0.028	0.028	1.333	1.333	0.7560
B240-T270-H_{mid}-X_{min}-1-14-L60 (12)	39.15-42.75	40.95	51.75	51.75	0.85	0.70	1.214	0.021	0.02	0.022	0.027	0.027	1.286	1.286	0.6986
B240-T240-H_{max}-X_{min}-1-14-L60 (16)	38.18-45.02	41.40	52.53	52.23	0.94	0.073	12.877	0.017	0.016	0.019	0.022	0.022	1.294	1.294	0.5745
B240-T240-H_{min}-X_{min}-1-14-L60 (17)	38.18-45.02	41.40	52.53	52.23	0.94	0.073	12.877	0.017	0.016	0.019	0.022	0.022	1.294	1.294	0.5745
B240-T240-H_{mid}-X_{min}-1-14-L60 (18)	38.18-45.02	41.46	52.56	52.26	0.94	0.073	12.877	0.017	0.016	0.019	0.022	0.022	1.294	1.294	0.5749

Table 12. T300, T270, T240 type single row bolt finite element model and comparison of experimental results.

Exp.	Resistance (kN.m)			Stiffness (kN.m/rad)			Rotation (rad)					Ψ_j	$\Psi_{j.max\ load}$	Energy dissipated (kN.m.rad)
	$M_{j.Rd}$	$M_{j.max}$	$M_{\theta Cd}$	$S_{j.ini}$	$S_{j.p-1}$	$S_{j.ini}/S_{j.p-1}$	$\theta_{M.Rd}$	$\theta_{min.K.R}$	$\theta_{Msup.k.R}$	$\theta_{Mj.max}$	θ_{Cd}			
4--4	4.21	3.84	3.87	1.98	1.74	1.16	0.44	1.44	0.49	0.40	0.40	0.90	0.90	1.54
5--5	4.86	3.07	3.07	0.33	2.35	0.14	3.91	8.21	0.54	0.47	0.47	0.12	0.12	1.44
6--6	5.11	3.10	3.10	1.81	1.39	1.31	0.60	4.60	0.51	0.34	0.34	0.57	0.57	1.05
10--10	7.97	3.42	3.42	0.15	1.38	0.11	10.00	9.52	1.40	0.28	0.28	0.03	0.03	0.98
11--11	13.70	3.70	3.70	0.96	1.43	0.68	1.50	1.82	0.39	0.28	0.28	0.18	0.18	0.51
12--12	10.72	3.30	3.47	3.40	0.99	3.47	0.62	0.71	0.43	0.35	0.34	0.55	0.56	1.18
16--16	4.93	3.12	3.14	1.25	0.17	7.57	0.29	0.80	0.17	0.14	0.14	0.48	0.50	0.45
17--17	3.53	3.92	3.92	0.67	1.03	0.66	0.89	2.08	0.34	0.35	0.35	0.39	0.39	1.37
18--18	4.61	3.13	3.18	0.56	0.18	3.13	0.63	0.59	0.28	0.28	0.28	0.44	0.45	0.88

4. Conclusions

Looking at the $M_{j.Rd}$ values; T300 largest value in the group appears to be in H_{max}-X_{min} group. Referring to these values in the group appears to be in the H_{min}-X_{min} group T270. With the increase of H value, BB value increased in all groups. The highest change was seen in the T270 group when the H_{max}-X_{min} and H_{min}-X_{min} groups were compared, an increase of 45.43%.

Considering A and B values; it is seen that the largest value of the T300 group is in the H_{mid}-X_{min} group. Looking at these values for the T270 and T240 groups, it is seen that they are in the H_{max}-X_{min} and H_{mid}-X_{min} groups. But the T240 in the combination group and H_{max}-X_{max} and H_{mid}-$X_{max\ group}$ have the highest. When all groups with an increase in the H value has increased the value of $M_{\theta Cd}$ and $M_{j.max}$. It is seen that H_{mid} values are higher than H_{min} values in T300 and T270 groups. The thickness of the combination should be selected types of joint's increases H_{mid}. $M_{\theta cd}$, the highest increases in the T240 group H_{max}-X_{min} and H_{min}-X_{min} group has been increased by %20.10. Likewise, this ratio is %20.58 in $M_{j.max}$.

T connection elements through the wall thickness increase stiffness reduction is observed. Data were seen to be the largest in the value H_{min} examined. So are the rigid connections. H_{max} or H_{mid} should be used to reduce stiffness.

References

Abdalla KM, Chen WF (1995). Expanded database of semi-rigid steel connections. *Computers & Structures*, 56(4), 553-564.

Aydın AC, Kılıç M, Maali M, Sağıroğlu M (2015a). Experimental assessment of the semi-rigid connections behavior with angles and stiffeners. *Journal of Constructional Steel Research,* 114, 338-348.

Aydın AC, Kılıç M, Maali M, Sağıroğlu M (2015b). Experimental investigation of sinus beams with end-plate connections. *Thin-Walled Structures*, 97, 35-43.

Batho C, Rowan H (1934). Investigations on beam and stanchion connections. *Second Report of the Steel Structures Research Committee*, London.

Coelho AMG, Bijlaard FS (2007). Experimental behaviour of high strength steel end-plate connections. *Journal of Constructional Steel Research*, 63(9), 1228-1240.

Díaz C, Victoria M, Martí P, Querin OM (2011). FE model of beam-to-column extended end-plate joints. *Journal of Constructional Steel Research*, 67(10), 1578-1590.

Kukreti AR, Zhou FF (2006). Eight-bolt endplate connection and its influence on frame behavior. *Engineering Structures*, 28(11), 1483-1493.

Maali M, Kılıç M, Aydın AC (2016). Experimental model of the behaviour of bolted angles connections with stiffeners. *International Journal of Steel Structures*, 16(3), 719-733.

Maali M, Kılıç M, Sağıroğlu M, Aydın AC (2017). Experimental model for predicting the semi-rigid connections' behaviour with angles and stiffeners. *Advances in Structural Engineering*, 20(6), 884-895.

Maali M, Aydın AC, Showkati H, Sağıroğlu M, Kılıç M (2018a). The effect of longitudinal imperfections on thin-walled conical shells. *Journal of Building Engineering*, 20, 424-441.

Maali M, Sagiroglu M, Solak MS (2018b). Experimental behavior of screwed beam-to-column connections in cold-formed steel frames. *Arabian Journal of Geosciences*, 11(9), 1-6.

Piluso V, Rizzano G (2008). Experimental analysis and modelling of bolted T-stubs under cyclic loads. *Journal of Constructional Steel Research*, 64(6), 655-669.

Shi G, Shi Y, Wang Y, Bradford MA (2008). Numerical simulation of steel pretensioned bolted end-plate connections of different types and details. *Engineering Structures*, 30(10), 2677-2686.

Tagawa H, Gurel S (2005). Application of steel channels as stiffeners in bolted moment connections. *Journal of Constructional Steel Research*, 61(12), 1650-1671.

Tagawa H, Liu Y (2014). Stiffening of bolted end-plate connections with steel member assemblies. *Journal of Constructional Steel Research*, 103, 190-199.

Tagawa H, Nagoya Y, Chen X (2020). Bolted beam-to-column connection with buckling-restrained round steel bar dampers. *Journal of Constructional Steel Research*, 169, 106036.